THESIS

FLOW DYNAMICS AND SCALAR TRANSPORT IN DRINKING WATER CONTACT TANKS

Submitted by

Taylor C. Barnett

Department of Civil and Environmental Engineering

In partial fulfillment of the requirements

For the Degree of Master of Science

Colorado State University

Fort Collins, Colorado

Spring 2013

Master's Committee:

Advisor: Subhas Karan Venayagamoorthy

Pierre Y. Julien

Hiroshi Sakura

ABSTRACT

FLOW DYNAMICS AND SCALAR TRANSPORT IN DRINKING WATER CONTACT TANKS

The research and studies presented in this thesis focus on ways to improve the internal hydraulics of chlorine contact tanks used in drinking water disinfection systems. This was accomplished through the use of computational fluid dynamics (CFD) and physical tracer studies of a number of different systems. Three primary tank modifications were investigated in these studies: internal baffling; inlet modifications; and random packing material. The findings from these studies were then applied in a case study of the Jamestown chlorine contact tank. All of the studies presented in this thesis use the baffle factor (BF) designation as defined by the United States Environmental Protection Agency as the primary indicator of a system's disinfection efficiency.

The CFD models used for the internal baffling study were first validated using a laboratory scale study of the Embsay chlorine contact tank in Yorkshire, England. This tank footprint was then modified to replicate a precast concrete tank that was installed in the Hydraulics Laboratory located at the Engineering Research Center (ERC) at Colorado State University. This concrete tank was used as the footprint for a parametric study in which the number and length of internal baffles were modeled in various configurations. The internal hydraulics of this baffle tank were optimized using only two dimensionless relationships namely: the baffle opening ratio L^* and the baffle opening to channel width ratio L_{bo}/W_{ch}. The resulting tank geometry from these two relationships yielded a BF of 0.80 and also maximized the length to width ratio of each channel within the concrete tank.

The inlet modification study was performed to investigate how the BF of a 400-gallon doorway storage tank could be improved. Three different inlet types with two inlet sizes were modeled and simulated for six different flow rates. Three of these CFD simulations

were then physically tested using both saline and lithium tracers to validate the computer models. Key findings from this study show that the size of the inlet and its orientation play a dominant role in the internal hydraulics of the system.

For the random packing material study, three different packing material sizes, two tank sizes, and two different flow rates were tested. CFD models were not feasible due to the randomness of how the packing material would settle in these contact tanks. Over 64 saline tracer studies and 6 lithium tracer studies were conducted to complete this study. Key findings show that the initial BF of the system and the volume of the tank filled with the packing material were the dominant variables in the study. The tank size, flow rate, and packing material size had little to no impact on the performance.

The Jamestown case study presented in this thesis used findings from both the internal baffle study and the inlet modification study. The BF of the contact tank would fluctuate annually between 0.52 and 0.63 due to a shift in flow regimes caused by a change in the system's flow rate. This turbulent to laminar flow regime change was validated with the use of CFD models coupled with physical tracer studies. Several inlet modifications were investigated using CFD to determine what modifications, if any, the plant operators should implement. Key findings from the CFD models showed that with the proper inlet modification, the BF of the system could be stabilized at 0.63 during both the high flow summer months and low flow winter months.

ACKNOWLEDGEMENTS

I would like to thank my advisor, Dr. Karan Venayagamoorthy for his support and guidance during both my undergraduate and graduate studies. Without his influence and help, none of this would have been possible. The guidance he gives to his students, and the enthusiasm he has in doing so, are unmatched. I enjoyed the challenges he has presented me with and I cannot thank him enough for how he has influenced my life. I would also like to acknowledge my committee members, Dr. Pierre Julien and Dr. Hiroshi Sakurai, for their help and support for this project.

Additionally I would like to thank my parents, Randy Barnett and Karen Rein, for their support. It was through their nurturing and sacrifices that I became the person I am today. Their constant words of support during my academic endeavors help give me the strength needed to continue on and persevere.

I would also like to thank the members of Dr. Karan's research group: Farid Karimpour, Ben Mater, Jordan Wilson, Kyung-Seop Shin, Jongseok Cho, Ali El-Turki, and Simon Schaad, for their support and help. I especially thank Justin Kattnig for his help in performing countless tracer studies.

Finally I would like to thank the Colorado Department of Public Health and Environment (CDPHE) Water Quality Control Division (Program Engineers: Tyson Ingles, Melanie Criswell, and Gordon Whittaker) for their continued support of this research project. Grateful acknowledgement is also given to the cities of Jamestown, CO and Tres Valles West, CO for the use of their respective systems.

TABLE OF CONTENTS

LIST OF TABLES

LIST OF FIGURES

Chapter 1

Introduction

1.1 Background

A key aspect of any civilization is easy access to safe and clean drinking water. In the United States, the Environmental Protection Agency (EPA) has been charged with the task of overseeing the water treatment processes to ensure it will be safe for human consumption. To help in this endeavor the EPA has allowed state run regulatory agencies to have oversight over the treatment systems within their state borders or have what is known as the "primacy". The Colorado Department of Public Health and Environment (CDPHE) has the primacy in the state of Colorado, and as such is responsible for regulating the quality of drinking water provided to its residents. However, guidelines established by the EPA are not often straightforward to regulate, especially with small drinking water supply systems. The research presented in this thesis will enable CDPHE to better regulate these small systems in Colorado.

1.2 Scope of Work

The research presented in this thesis represents the fourth phase of a four-phase project that was sponsored by the Water Quality Control Division of CDPHE. The first phase of this project was completed by Qing Xu as part of her masters thesis entitled *Internal Hydraulics of Baffled Disinfection Contact Tanks using Computational Fluid Dynamics*. Jordan Wilson completed the second phase of the project as part of his masters thesis entitled *Evaluation of Flow and Scalar Transport Characteristics of Small Public Water Disinfection Systems using*

Computational Fluid Dynamics, while Zach Taylor completed phase three and part of phase four with his masters thesis entitled *Towards Improved Understanding and Optimization of the Internal Hydraulics of Chlorine Contact Tanks*. The scope of work for the fourth phase of this project includes the following:

1. Phase 4a: Baffle Factor Modeling
    (a) Perform computer modeling of tank configurations that simulate poor, average, and superior baffling as described in Table 2.1 (See Chapter 2):
        i. Produce a project plan outlining modeling scenarios.
        ii. Generate computer models for the agreed upon configurations.
    (b) Provide an oral and written presentation to CDPHE engineers on the findings from Phase 4a.
2. Phase 4b: Small System Disinfection Contact Basin Modification Project
    (a) Design, build, and test a rectangular tank that can be physically modified to validate the models developed in Phase 4a. Tracer studies should be performed at multiple flow rates.
    (b) Outreach to participating public water systems to provide tank modifications and baffling factor tracer studies to verify baffling factor conditions before and after tank modifications are made.
    (c) Provide an oral and written presentation to CDPHE engineers on the findings from Phase 4b.
3. Phase 4c: Guidance Document
    (a) Develop a guidance document to address overall baffling factor issues and provide effective contact basin design guidance. This guidance document will address:

i. Assessing the adequacy of the existing baffling factor criteria in Long Term 1 Enhanced Surface Water Treatment Rule (LT1ESWTR) *Disinfection Profiling and Benchmarking Technical Guidance Manual*,

ii. Investigating and evaluating the effect of several factors on the overall disinfection contact time, including, but not limited to:

   A. Basin geometry

   B. Inlet/outlet configurations (e.g. location and sizing)

   C. Inlet/outlet design (e.g. velocity)

   D. Intra basin baffling configurations

   E. Other modifications (addition of media, etc.) to increase baffling factors

   F. Water quality parameters (e.g. temperature)

iii. Developing baffling factor determinations for typical basin design configurations.

iv. Provide cost effective recommendations of disinfection contact basin design.

1.3 New Contributions

The research presented in this thesis has yielded the following new contributions:

- Refined the design guidelines for the construction of serpentine baffle contact tanks with sharp inlets. These guidelines optimize the baffling factor of the contact tank using the tank width, tank length, baffle opening, and baffle channel width.

- The applicability of using internal packing material to improve the hydraulic efficiency of a contact tank. Initial tests showed that with the use of this packing material, a baffling factor of up to 0.9 can be achieved.

- Validity of using computer models to design modifications to existing contact tanks.

1.4 Research Publications

An abstract titled, *Computational Modeling and Experimental Testing of Disinfection Contact Tanks* has been accepted to the 2013 World Environmental and Water Resources Congress. This research will be presented under the Hydraulics and Waterways (Computational Hydraulics) section of the conference. Chapter 4 is currently being prepared for submission to Journal of Environmental Science and Technology. The research presented in Chapter 5 on the use of packing material is currently being prepared for submission to Journal of American Water Works Association.

1.5 Organization of Thesis

Chapter 2 consists of a literature review that helps provide a background upon which the research presented in this thesis will build upon. This chapter highlights some problems inherent in small drinking water systems and also provides an explanation of the CT method used to determine log inactivation values for different microbiological contaminants. The turbulence model and commercial software that were used in this thesis are also discussed.

Chapter 3 presents a parametric serpentine baffle study in which the number of baffles and baffle length were varied for a given tank foot print in order to optimize the internal hydraulics of the contact tank. Chapter 4 highlights a subtle issue of turbulent to laminar transition in contact tanks and how this can adversely affect the hydraulic efficiency of the system. This chapter consists of several computer model simulations of the Jamestown contact tank, along with tracer studies used to validate the simulation results. Chapter 5 analyzes the effects of inlet modifications and internal packing material. This chapter utilizes several water storage tanks that small drinking water systems typically use. The packing materials presented in this chapter are shown to have the capability of increasing the baffling factor of the tanks used to values over 0.9.

Chapter 2

Literature Review

2.1 Small Drinking Water Systems

Small water sterilization systems account for approximately 92% of the 51,988 total community water systems (CWS) in the United States EPA (2011). These small CWSs provide drinking water for populations up to 10,000 people, however 90% of the 47,856 small CWSs serve 3,300 people each or fewer. While these small CWSs only provide water for 18% of the population, their violations account for 94% of all violations for CWSs EPA (2011). These violations are primarily monitoring and reporting (M&R) issues, but small CWSs still account for 93% of all violations in maximum contaminant levels (MCLs). Often, the small CWSs have part time plant operators and may face other technical, managerial, and financial issues that larger plants do not encounter.

A crucial aspect of plant operation is to determine the baffle factor (BF) of the disinfection contact tank. This baffle factor is used in the CT calculations for water disinfection. A table for visually determining baffle factors is found in the LT1ESWTR *Disinfection Profiling and Benchmarking Technical Guidance Manual*. Many times a small CWS can only estimate the BF of their contact tank with this manual, while larger systems determine their BF with the use of computational fluid dynamics (CFD) and/or tracer studies. The method of visually determining the baffle factor from the manual can be highly ineffective, and as such generally gives the system a higher BF. The research in this thesis will help CDPHE be able to better advise small CWSs on how to improve the efficiency of their contact systems.

2.2 Water Disinfection

In the United States, the Safe Water Drinking Act (SWDA) mandates that all drinking water meet certain criteria in order for it to be deemed potable. Enforcement of these criteria can be handled by either the EPA, a state regulatory agency (i.e. CPDHE), or a Native American Tribe EPA (2004). Currently Wyoming and the District of Columbia are the only two locations in which the EPA is directly responsible for water quality enforcement. The National Primary Drinking Water Regulations (NPDWR) and National Secondary Drinking Water Regulations (NSDWR) list the maximum permissible limits of various contaminants in drinking water. Of these regulations the two of most interest are giardia and cryptosporidium. These two microbiological contaminants are responsible for the majority of water borne illnesses, with over 430,000 cases being reported between 1980 and 1996 Davis (2008).

Drinking water can be disinfected by numerous means (e.g. chlorine, chlorine dioxide, ozone, chloramines, UV radiation), however chlorination has become the most common method (Wang *et al.*, 2003). Microbial inactivation methods like these are usually the most effective way to kill pathogenic microorganisms that may be present in the raw drinking water (Baawain *et al.*, 2006). The CT method is used to ensure that the water has been safely disinfected. This method gives a measure of the disinfection concentration in the effluent (C) and how long it was in contact with any contaminants in the water (T). While the disinfectant concentration is easy to measure with water samples at the outlet, the contact time, T, is much harder to quantify. The first step in determining the contact time is to calculate the theoretical detention time (TDT) of the tank. This theoretical detention time is calculated by dividing the lowest volume of water the tank will contain during normal operation by the peak hourly flow rate. The calculation of TDT assumes the tank has perfect plug flow. In perfect plug flow, there is no short-circuiting or recirculation within the tank and every parcel of water stays in the tank for the same amount of time. Since this is almost

never the case, a correction coefficient called the baffling or baffle factor is used to reduce the TDT to a value more realistic of the tank. This baffle factor can be calculated by the use of Equation 2.1. In Equation 2.1, T_{10} is the time at which 10% of the given tracer concentration is observed at the outlet. In the absence of a tracer study, the BF of a contact tank can be visually estimated using Table 2.1. However this method tends to greatly over or under estimate the performance of a contact tank as the descriptions are very broad and vague. Once the BF, TDT, and residual disinfectant concentration (C) are known, the CT_{Calc} can be calculated using Equations 2.2 and 2.3. Then the log inactivation can be determined by using the tables in the manual to determine the $CT_{99.9}$ or $CT_{99.99}$ that are needed for 3 or 4 log inactivation.

$$BF = \frac{T_{10}}{TDT} \tag{2.1}$$

$$T = TDT * BF \tag{2.2}$$

$$CT_{Calc} = C * T \tag{2.3}$$

Table 2.1: Baffling classification from LT1ESWTR *Disinfection Profiling and Benchmarking Technical Guidance Manual*

Baffling Condition	T_{10}/TDT	Baffling Description
Unbaffled (mixed flow)	0.1	None, agitated basin, very low length to width ratio, high inlet and outlet flow velocities.
Poor	0.3	Single or multiple unbaffled inlets and outlets, no intra-basin baffles.
Average	0.5	Baffled inlet or outlet with some intra-basin baffles.
Superior	0.7	Perforated inlet baffle, serpentine or perforated intra-basin baffles, outlet weir or perforated launders.
Perfect (plug flow)	1.0	Very high length to width ratio (pipeline flow), perforated inlet, outlet, and intrabasin baffles.

2.3 Tracer Studies

Tracer studies provide statistical measurements of the complex flows found within contact tanks. If properly conducted they can provide a much more accurate BF than those determined visually with the help of Table 2.1. In addition to determining the BF of contact tanks, they are crucial for validating CFD models. In these studies a conservative or non-reactive material is injected into the influent of a tank. Several varieties of tracer solutions (saline, fluoride, lithium, rhodamine WT) are commercially available, however only saline and lithium studies were performed for this research. Saline was used for the low cost of the solution, while lithium was used for its accuracy due to the low background concentration found in raw water.

2.3.1 Pulse Input

In a pulse input tracer study a large quantity of tracer is injected into the influent in a very short span of time. Generally, this injection time should be no longer than 1% of the TDT to avoid inaccurate results Wilson (2011). The tracer concentration is then monitored in the effluent so that a break through curve can be obtained. This break through curve is known as a flow through curve (FTC) and resembles something similar to a probability density function (PDF) as shown in Figure 2.1. This figure was created with data from a CFD model of a hypothetical contact tank. FTCs are often plotted with the normalized tracer concentration of the y-axis and t/TDT on the x-axis to aid in reading the results. This also allows for FTCs to be easily compared, whether they are from different systems or the same system at multiple flow rates.

While this type of tracer study is generally easier to perform it does have several shortcomings. The first of which involves the introduction of the tracer to the influent. In a pulse tracer study, the stock tracer solution that is mixed with the influent needs to be highly

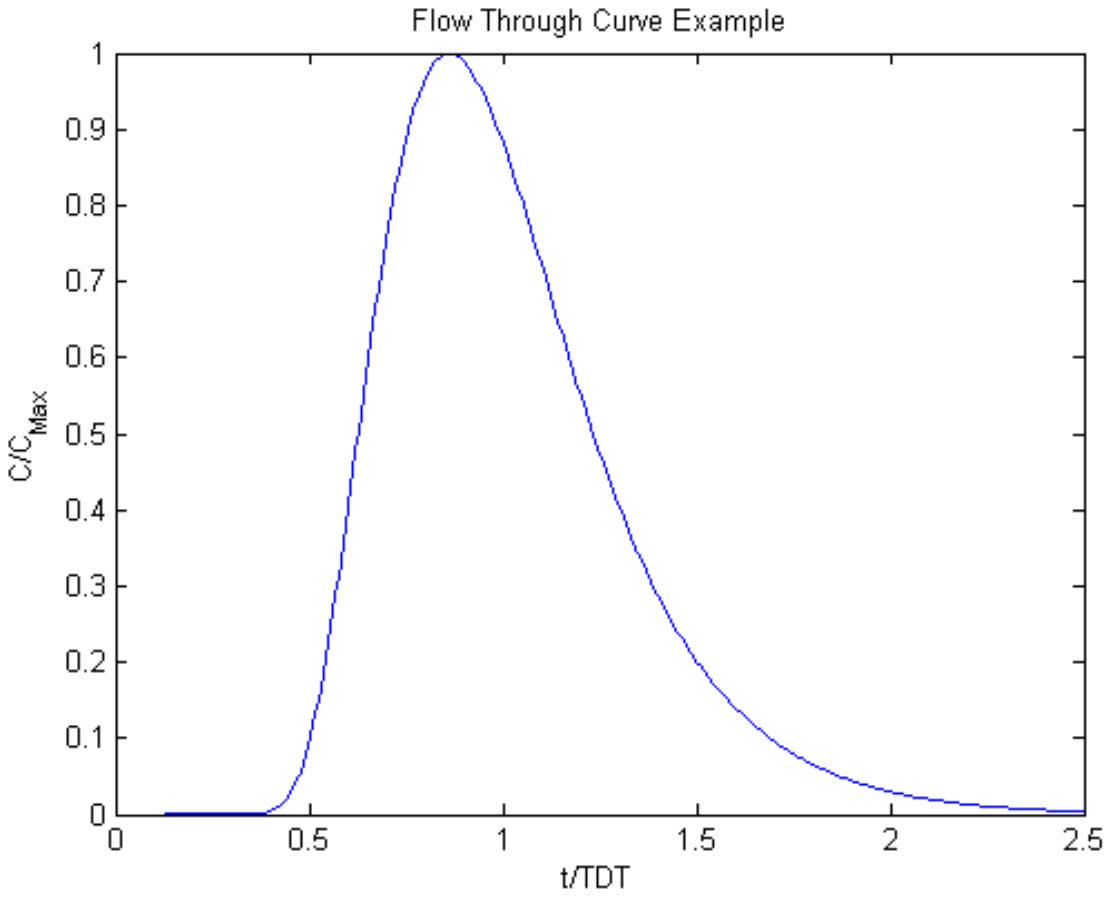

Figure 2.1: Example of a flow through curve

concentrated so that it can be injected quickly. If the solution does not fully mix with the influent the sharp peak seen in Figure 2.1 will flatten out. Another shortcoming of a pulse tracer is that if the peak of the rising limb in Figure 2.1 is not properly captured it will skew the calculations of the *BF*. Despite these issues, a pulse study has several advantages over a step input study. In a pulse input study the mass of tracer recovered can be calculated from the FTC and checked with the initial amount injected. Another advantage of the FTC is that the mean residence time of the tracer in the contact tank can be determined much easier. A pulse input tracer study is also much easier to perform on large systems with a high *TDT*. In these large systems a step input study would require a large amount of solution, which is not always practical.

2.3.2 Step Input

Unlike a pulse input tracer study, the tracer in a step input study is continuously injected during the entire test. This allows for a much lower concentration of stock tracer solution to be used, which minimizes any issues of the solution not being fully mixed in the influent. In a step input tracer study the tracer concentration is continuously measured in the effluent until it reaches a steady state. When the break through curve of a step input study is plotted it yields the residence time distribution (RTD) curve. Figure 2.2 shows an example of a RTD curve of a system. This RTD curve resembles something similar to a cumulative distribution function (CDF), which has several advantages over the FTC generated by the pulse study.

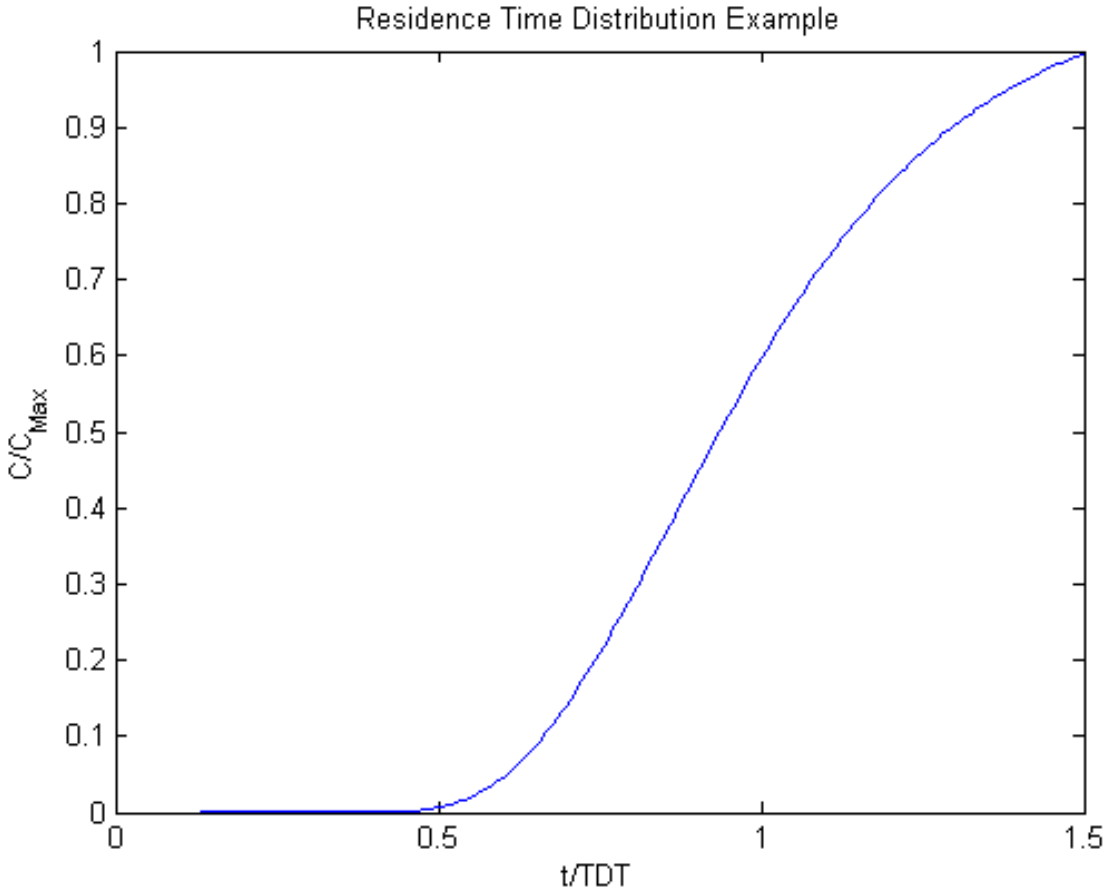

Figure 2.2: Example of a residence time distribution curve

Much like in a FTC, RTD curves are often plotted with the normalized tracer concentration on the y-axis and t/TDT on the x-axis. However due to the shape of a RTD curve, the baffle factor of the system or systems plotted can be read directly from the graph. Another advantage of a step input tracer study is that two studies can be performed in one test. This is accomplished by monitoring the falling tracer concentration at the outlet once the system has reached steady state and the tracer feed at the inlet has been shut off. This falling RTD curve looks very similar to the one shown in Figure 2.2 except the tracer concentration starts at 1 and falls to 0. These step input studies are generally easier to conduct on an existing system while it is in operation as well. Many times existing chemical feeds can be utilized to inject the tracer solution into the influent due to the slow tracer injection rate. However, these benefits come at a cost. Since the step input method requires that the tracer be continuously injected during the entire test, a larger amount of solution is needed than in a pulse study. Another issue is that there is no reliable way to calculate the mass of the tracer recovered for comparison with what was injected. All of the tracer studies conducted for the research presented in this thesis used the step input method as it was easier to obtain the BF from the raw data.

2.4 Commercial Software

2.4.1 Solidworks

In the last ten to fifteen years, computer aided design (CAD) programs have become much more intuitive and user-friendly. Currently two of the most popular CAD programs for three-dimensional modeling are Pro/ENGINEER by PTC and SOLIDWORKS by DASSAULT SYSTEMES. While ANSYS Workbench includes a three-dimensional geometry modeler it was not used in this study, as it is very cumbersome and difficult to use. SOLIDWORKS was used to create all of the model geometries for the various studies found in this thesis. Since

many companies that use FLUENT also use a different CAD program than the one provided in Workbench, ANSYS allowed its' geometry modeler and meshing programs to read various proprietary CAD file formats. Since the SOLIDWORKS platform was much easier to learn and use, than the one provided with Workbench, it was chosen as the primary CAD program. These SOLIDWORK files were saved using the DASSAULT SYSTEMES proprietary file extension ".stlprt" and directly imported into the Workbench meshing program provided by ANSYS.

2.4.2 FLUENT

ANSYS FLUENT Version 13 was used as the primary CFD program for the research presented in this thesis. FLUENT uses a finite-volume discretization of the Reynolds Averaged Navier-Stokes (RANS) equations coupled with an unstructured mesh to compute the flow dynamics within a given computational domain. This unstructured mesh allows for much easier mesh creation, especially with complicated geometries. Unlike the structured mesh used by FLOW-3D, the cells created for FLUENT are fitted to the solid body being meshed. This helps to ensure that the geometry being meshed is accurately portrayed. This body fitted mesh also helps avoid any "stair step" or other non-realistic geometry representations that are inherent to orthogonal meshes. In an orthogonal mesh, like that used by FLOW-3D, proper resolution near the boundaries of solid bodies is crucial. In these structured orthogonal meshes, the shape of the solid bodies is preserved by interpolating where the solid body crosses through each cellblock. While this yields little to no errors when interpolating rectangular bodies, inaccurate mesh resolution of circular or arced bodies will yield poor results. This phenomenon is most easily described by how the mesh would depict a circle. If a circular body only encompasses four cell blocks in a structured orthogonal mesh, then the circular body will be seen as a square body by the solver. Since the mesher would only have four points to interpret this body from, it would incorrectly give the solver function in

the CFD program a square body. As more cells are added to this mesh, the circular body would begin to look more like a circle and less like a square.

While the unstructured mesh has several advantages, it is not without its faults. One draw back from this type of mesh is the computational time required to access the mesh during simulation calculations. In a structured mesh each cellblock can be identified by three indices (i,j,k). For unstructured meshes a much more complicated scheme is needed to identify cellblocks. Another shortcoming in FLUENT is the lack of a robust two-phase modeler. While the VOF method used by FLUENT works fine if the simulation is with two liquids, this VOF method becomes very diffusive in liquid/gas simulations. This diffusive boundary between the liquid/gas interface is mainly due to the interpolation schemes used by FLUENT.

2.4.3 FLUENT Methodology

All simulations performed in FLUENT used only a single-phase model with a rigid lid assumption. This assumption allowed the free surface of the water to be modeled by a symmetry boundary. A constant velocity with the appropriate turbulent kinetic energy (k) and turbulent kinetic energy dissipation rate (ϵ) were specified at the inlet, and varied depending on the size of the inlet and the flow-rate of the system. All of the walls had a no-slip condition prescribed with the enhanced wall-function while the outlet was treated as a pressure outlet discharging to the atmosphere. These simulations were then performed in two separate steps. First, the first order upwind steady-state solver with the RNG turbulence model was used to converge on the turbulent steady-state velocity field. Once convergence was achieved, the transient-state solver was used with a 3 second time step so that the passive scalar could be tracked through the system in time. The tracer concentration was modeled using the advection-diffusion equation given by:

$$\frac{DC}{Dt} = \frac{\partial C}{\partial t} + \overline{U} \cdot \nabla C = \nabla \cdot \left(\left(\kappa + \frac{\nu_t}{Sc_t} \right) \nabla C \right) \tag{2.4}$$

where: C is the concentration of tracer; $\overline{U}$ is the transient-state velocity; κ is the molecular diffusivity of the tracer; ν_t/Sc_t is the turbulent diffusivity of the tracer with ν_t being the turbulent eddy viscosity and Sc_t is the turbulent Schmidt number Wilson & Venayagamoorthy (2010). In Equation 2.4 both $\overline{U}$ and ν_t were determined from the transient-state simulation results while the turbulent Schmidt number(Sc_t) was taken as 0.7 Venayagamoorthy & Stretch (2010). Appendix A shows the User Defined Function that was used by FLUENT to solve for the total diffusivity of the passive scalar.

2.4.4 FLOW-3D

FLOW-3D by FLOW Science is a finite difference computational fluid dynamics (CFD) program coupled with a structured orthogonal mesh. This program offers a very robust two-phase model called truVOF$^{\text{TM}}$ and a fractional area volume obstacle representation (FAVOR$^{\text{TM}}$) that are used in combination during a simulation. While the finite difference discretization of the Reynolds Averaged Navier-Stokes equations do not guarantee the conservation of mass or momentum, both of these important characteristics are preserved in FLOW-3D simulations. FLOW-3D accomplishes this by how the structured orthogonal grid is utilized in tandem with the finite difference Navier-Stokes equations. When the Navier-Stokes equations are discretized and applied to a mesh in a CFD program, they are no longer partial differential equations (PDE's). Instead, they become a simple algebraic system of equations. This system of equations is then solved iteratively until the specified convergence criteria are reached. The algebraic system of equations that is solved by FLOW-3D is identical to those created when the Navier-Stokes equations are discretized using a finite-volume method and then applied to an unstructured mesh. Since the orthogonal mesh coupled with the finite-difference method yields the same results as the finite-volume method, the

conservation of both mass and momentum are guaranteed.

One of the main advantages of FLOW-3D is its two-phase modeling capabilities. While many CFD programs have a two-phase volume of fluid (VOF) method, they do not perform nearly as well as the truVOF^{TM} used by FLOW-3D. In a VOF simulation each mesh cellblock is assigned a fluid fraction (F) between 0 and 1 (FLOW Science, 2012). A cellblock with an F value of 1 would contain only liquid while a block with a value of 0 would contain only gas or a different type of liquid. The free surface between the two fluids can then be extrapolated with these F values. One reason FLOW-3D is able to handle two phase simulations is how this interface is calculated from the mesh. In an unstructured tetrahedral mesh (like that found in FLUENT) it is difficult to accurately define a sharp interface between fluids. Complicated algorithms are needed to compute the fluid/fluid interface from the F values due to the obscure shape the elements have in these tetrahedral meshes. Since FLOW-3D has a very simple structured orthogonal grid, it is very easy to interpolate where the fluid/fluid interface is located using only the F values of the surrounding cells. Another reason FLOW-3D has a more accurate VOF method is how it handles a liquid/gas simulation. When a simulation in FLOW-3D contains both a gas and a liquid, FLOW-3D does not perform any calculations in cells containing only gas (FLOW Science, 2012). Since gases have densities that are orders of magnitude smaller than liquids, this omission causes little error and in actuality it does quite the opposite. When a RANS CFD code uses a VOF method, it will calculate the average parameters (velocity, turbulence quantities, pressure, etc.) for each cell. In a cell with only liquid these average parameters would be an accurate representation for the properties of the fluid flow. However for cells that are near the fluid interface these average parameters would be inaccurate as the CFD program would incorrectly assume that the liquid and gas are moving at the same speed.

While FLOW-3D may have superior two-phase modeling capabilities, it is not without shortcomings. One such shortcoming is that the simulation run times are significantly longer than those required in FLUENT. Even with a simple one-phase model, FLOW-3D takes at

least 3 times longer than the same simulation would in ANSYS FLUENT. This is due to the FAVOR^{TM} employed in FLOW-3D. When FLOW-3D advances a simulation forward in time the FAVOR^{TM} method is used to determine how much of a cell is occupied by liquids, gases, and solids. This is computed for every cell in the mesh. The solids (walls, moving objects etc.) and fluid interface are then recomputed before the new velocity field is calculated. These extra steps significantly increase the computational burden and result in longer simulation times.

2.4.5 FLOW-3D Methodology

While the FLUENT simulations were limited to a single-phase model with a rigid lid assumption, those performed in FLOW-3D used a two-phase model. This was due to the powerful volume-of-fluid (VOF) and fractional area volume obstacle representation (FAVOR^{TM}) methods that FLOW-3D utilizes during a two-phase simulation. A constant volume flow rate with the appropriate turbulent kinetic energy (k) and turbulent kinetic energy dissipation rate (ϵ) were specified at the inlet while the outlet was treated as a pressure outlet discharging to the atmosphere. Both the inlet and outlet had a specified fluid fraction of 1 so only water was allowed to enter or leave the computational domain. After the geometry and mesh blocks of the simulation were created, a global fluid elevation was used to initialize the simulation. This allowed for a much shorter computational time since the computer would not need to waste time filling the computational domain with fluid.

To solve the mean flow equations, the k- ϵ RNG model with a no-slip wall boundary condition was used. To ensure the simulation would be accurate enough to model scalar transport, the second order monotonicity preserving scheme was used for the momentum advection equation. The simulation was then allowed to run until a steady state was reached. FLOW-3D considered the simulation to be at a steady-state when the total mass, average mean kinetic energy, average mean turbulent energy, and average mean turbulent dissipation

all varied less that 0.5% over a time window of 300 seconds. When FLOW-3D converges on a steady-state solution, the flow within the domain in not in a truly "steady state" instead it is in a quasi-steady state. This is because FLOW-3D only monitors the average residuals of the flow within the computational domain. In a quasi-steady state flow there can be non-steady state flow features like eddies or vortex shedding, however these features are well established and do not change their behavior over time.

Then a passive scalar with a nondimensional concentration of 1 was introduced at the inlet. The time step size was not specified since FLOW-3D automatically controlled this variable so that convergence would be guaranteed as the model progressed in time. FLOW-3D simulates passive scalars using an advection-diffusion equation similar to the one used by FLUENT, however no extra User Defined Function is needed to define the total diffusivity of the tracer. Instead a turbulent diffusion multiplier for the scalar species is used. Equation 2.5 shows the advection-diffusion equation used by FLOW-3D to model scalar transport.

$$\frac{DC}{Dt} = \frac{\partial C}{\partial t} + \overline{U} \cdot \nabla C = \nabla \cdot \left((\kappa + \nu_t M) \nabla C \right) \tag{2.5}$$

Where: C is the concentration of tracer; $\overline{U}$ is the transient-state velocity; κ is the molecular diffusivity of the tracer; M is the turbulent diffusion multiplier for the scalar species; and ν_t is the turbulent eddy viscosity. In Equation 2.5 both $\overline{U}$ and ν_t were determined from the transient-state simulation results while M was set to be the inverse of the turbulent Schmidt number (Sc_t) and was taken as 1/0.7 or 1.428 Venayagamoorthy & Stretch (2010).

2.5 Turbulence Model

While numerous turbulence models are available on a variety of CFD programs, only the renormalization group (RNG) k-ϵ model was used in the research presented. The RNG k-ϵ model is a relatively new two equation model that was developed by Yakhot and Orszag

at Princeton University Versteeg & Malalasekera (2007). This k-ϵ model "systematically removes the small scales of motion from the governing equations by expressing their effect in terms of larger scale of motions and a modified viscosity" Versteeg & Malalasekera (2007). The RNG k-ϵ model also differs from the standard k-ϵ model in the way it handles the turbulent Prandtl Number. The Prandtl Number is the ratio of turbulent or eddy viscosity to turbulent diffusivity Pope (2010). In the Standard k-ϵ model this turbulent Prandtl Number is merely a "... user-specified, constant value" while the RNG model calculates the turbulent Prandtl Number with an analytic equation (ANSYS, 2011). One of the important features of the RNG k-ϵ model utilized by the research presented in this thesis, was its ability to handle swirling flows with both high and low Reynolds Numbers (ANSYS, 2011). The ability to handle flows of high and low Reynolds Numbers was primarily used in the baffle study found in Chapter 3, while the ability to handle flows with lots of swirling and mixing was utilized in Chapter 5. The RNG k-ϵ model also includes an additional term in the calculation of ϵ. This additional term is not derived from the RNG theory and is the primary source of difference in the performance between the Standard and RNG k-ϵ models Pope (2010). These differences in how the RNG handles turbulence make it applicable to a much wider array of flows than the Standard k-ϵ model (ANSYS, 2011).

2.6 CFD Code Model Validation

To verify that both FLUENT and FLOW-3D would yield accurate results they needed to be compared with a benchmark case. A laboratory scale of the Embsay Chlorine Contact Tank in West Yorkshire, England was used for the benchmark test case as validation data was easily available thanks to Shino *et al.* (1991). Since the data from Shiono *et al.* included the average flow depth within the tank, a single-phase model could be run in FLUENT. Figure 2.3 shows the computational domains for both FLUENT and FLOW-3D. It should be noted that in Figure 2.3b the FAVOR^{TM}used by FLOW-3D has already added the fluid

into the tank. The tank had a flow depth of 0.536 meters and was 1.995 meters long by 0.94 meters wide. The contact tank also included seven baffles that were 0.045 meters thick and 0.75 meters long. Water was introduced into the tank by an inlet channel that consisted of a long straight section followed by a 90° bend into a short wider section. The long section of the inlet canal was 0.125 meters wide by 0.086 meters deep while the short section was 0.21 meters wide by 0.086 meters deep and 0.536 meters long. The tank outlet canal was 0.21 meters wide by 0.021 meters deep. A continuous flow rate of 1.17 x 10^{-3} m^3/s was modeled to match the experiments performed by Shiono *et al.* (1991). This flow rate leads to a theoretical detention time (TDT) of 774 seconds.

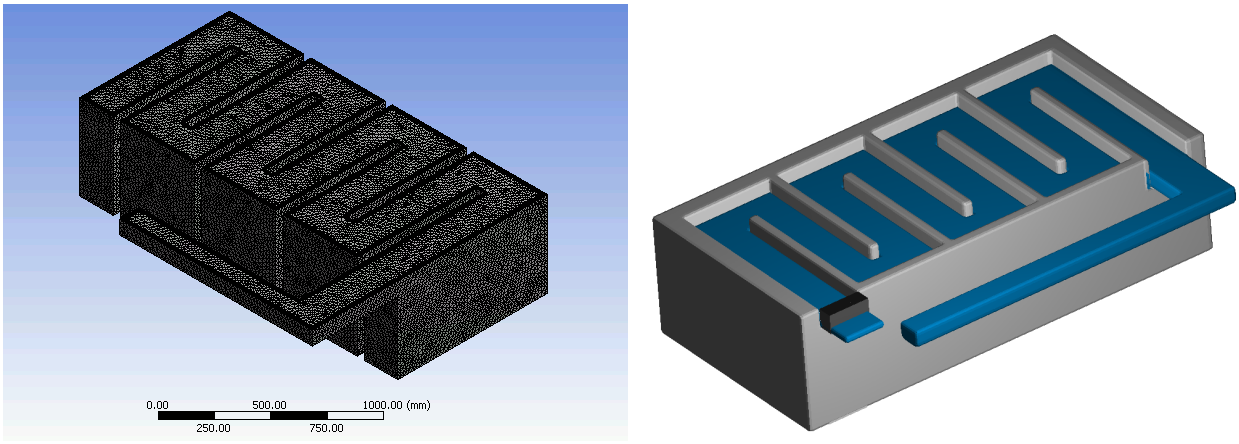

(a) FLUENT geometry **(b)** FLOW-3D geometry

Figure 2.3: Benchmark geometries

2.6.1 FLUENT Model

Using the measurements found in the previous section, a three-dimensional model of the Embsay contact tank was created in Solidworks for the FLUENT simulation. This geometry was then imported into ANSYS Workbench so it could be meshed. Several different meshes were created to ensure that the mesh used for the final simulation could accurately calculate the flow fields found in the real tank. These meshes ranged from 25,686 cells to 1,208,421 cells. An inflation layer was also defined on the walls of the tank so that the enhanced

wall function in FLUENT could be used. Once these meshes had been generated they were used to perform a parametric study to determine which one, if any, would be the optimal mesh. To achieve this, each mesh was allowed to run to a steady state solution after the proper boundary conditions had been applied. Next, the maximum velocities found in each simulation were plotted against the total number of cells in each mesh as shown in Figure 2.4. From this figure, it was decided that the mesh with 514,884 cells had sufficient resolution to accurately calculate the flow dynamics found in the Embsay contact tank.

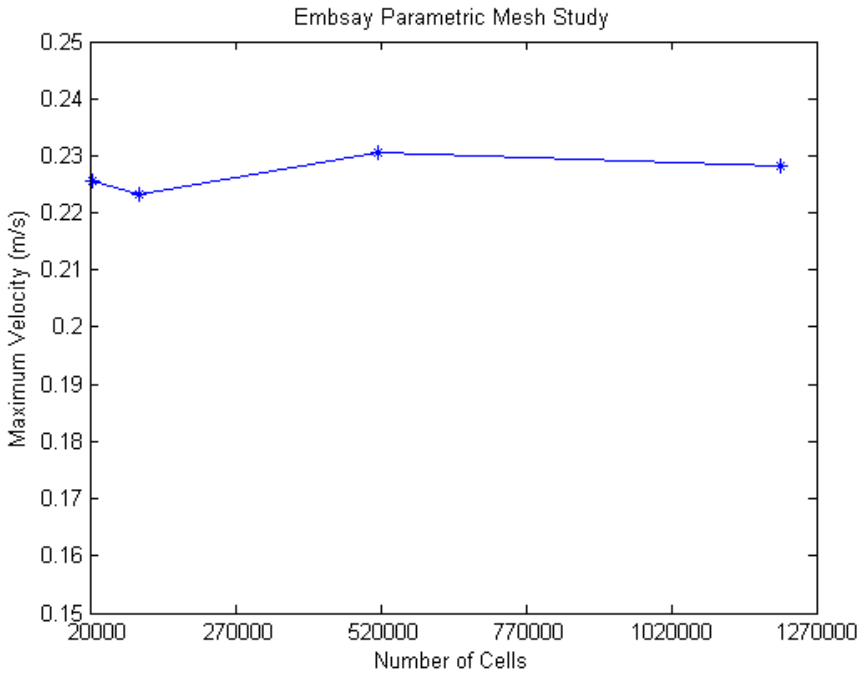

Figure 2.4: Maximum velocities from the mesh parametric study

With the mesh properly sized, a tracer study on the Embsay contact tank was then simulated using FLUENT. This simulation was first allowed to reach a steady state as discussed in Section 2.4.3 before a transient model was used. Once the transient model had been initiated, a non-dimensional passive scalar with a concentration of 1 was introduced at the inlet for 15 seconds to mimic the experiments by Shiono *et al.* Shiono *et al.* (1991). A monitor was placed on the outlet of the tank during this simulation so that the FTC of the system could be plotted. This simulation was then allowed to run for a flow time of 2.5

TDT. While a FTC can help demonstrate the internal hydraulics of a tank, it is difficult to determine the baffle factor of a tank directly from them, as discussed in Section 2.3.1. To aid in the calculation of the baffle factor, the FTC curve was integrated into a RTD curve as shown in Figure 2.5.

These two graphs behave very similar to a probability density function and a cumulative distribution function. As such Equation 2.6 below can be used to integrate a FTC into a RTD curve Taylor (2012). It should be noted that Figure 2.5b has been truncated to a final time of 1.5 *TDT*. This was performed so that the CFD data would depict the RTD curve over the same time span as the experimental results. As Figure 2.5 shows, FLUENT was able to accurately recreate the Embsay tank and predicted a baffle factor of 0.66 compared to the experimental baffle factor of 0.69. The simulation with a mesh size of 514,884 cells took approximately 30 minutes of computational time on a desktop computer with a i7 processor and 8 GB of RAM.

$$\frac{1}{C_0 * T_{release}} * \int_0^t FTC(t)\,\mathrm{d}t \approx \frac{RTD(t)}{C_0} \tag{2.6}$$

2.6.2 FLOW-3D Model

Since FLOW-3D defines the volume the fluid occupies in a different manner than FLUENT, a separate geometry was constructed using the FLOW-3D Geometry tab. When a geometry is created for a simulation in FLUENT the volume in which the fluid occupies is what is modeled as shown in Figure 2.3a. In FLOW-3D the exact opposite is true and a fluid can only occupy volumes that do not contain any solid objects. This meant that the geometry used in FLOW-3D simulations look more similar to the physical system as shown in Figure 2.3b. Once the geometry had been created so that it was compatible with FLOW-3D it was then meshed using the FLOW-3D Meshing tab. This mesh consisted of four mesh blocks that were connected by no more than one face. To ensure that the mesh blocks accurately

captured the walls and baffles of the tank, mesh planes were used. These mesh planes were also used to help line up the mesh cells at the interfaces of the mesh blocks. This mesh consisted of 644,208 cells in which the fluid could occupy and had a maximum aspect ratio of 1.5. After the model had been meshed, appropriate boundary conditions were applied to the walls of the mesh blocks. Unlike in FLUENT, surfaces within the mesh cannot be specified as inlets or outlets, instead the mesh block boundaries assume this function.

Due to the extra time involved in creating an accurate mesh in FLOW-3D, a parametric mesh study was not performed. It was assumed that if the results of the simulation matched those of FLUENT's and the experimental data, that the mesh would be sufficient. Figure 2.5 shows both the FTC and RTD for the FLOW-3D simulation, which was also able to accurately mimic the tracer study results from the Embsay contact tank. As Figure 2.5b shows, FLOW-3D predicted a baffle factor of 0.71, which was very close to the experimental results of 0.69. However, this increased accuracy FLOW-3D had in predicting the baffle factor came at a high computational cost. While the FLUENT simulation was able to run to completion in just over 30 minutes, the FLOW-3D simulation took over 1.5 days on an i7 CPU with 8 GB of RAM. The additional computational time was most likely the result of the FAVOR method. Each time FLOW-3D advances a simulation forward in time the FAVOR method has to re-render the mesh to define the solid areas. Once it has redefined the solid areas of the mesh, FAVOR then computes the fractional VOF in each mesh cell. Only after the FAVOR method has determined the solid areas and the new fractional VOF of each cell will it begin to perform the calculations for the next time step.

2.6.3 Conclusions

After both of the CFD codes had been validated, it was decided that only FLUENT would be used for the parametric studies presented in this research, while FLOW-3D would be used to calculate the initial water surface level only. FLOW-3D was not used for any parametric

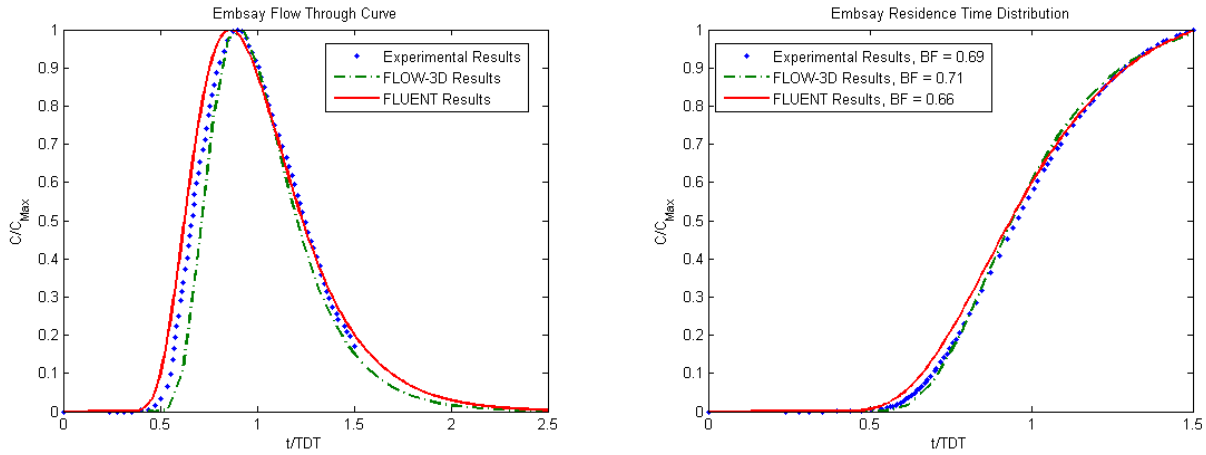

(a) Flow through curves **(b)** Residence time distribution

Figure 2.5: Validation graphs for FLUENT and FLOW-3D

studies due to the long computational time that the program required for each simulation. As Figure 2.5b shows, the rigid lid assumption used by FLUENT caused little error, while greatly reducing the computational time needed.

Chapter 3

Serpentine Baffle Tank Study

3.1 Introduction

Dead zones, eddies, and short circuiting within a drinking water contact tank are known to have negative effects on the tank's performance. Internal baffling within large, rectangular contact tanks has been shown to help reduce the occurrence of these anomalies by Amini *et al.* (2010) and Baawain *et al.* (2006). To ensure water is safe for human consumption, chlorine or another suitable disinfectant is added into the influent of a drinking water contact tank. The amount of chlorine required to effectively treat the water varies depending upon, among other things, the baffle factor and the detention time of the tank. An efficient contact tank would have a high baffle factor, which would allow for a lower dose of chlorine to be used. This is a desirable quality in contact tanks, as high doses of chlorine raise the risk of disinfection by-products (DBPs) in the effluent. These DBPs have been shown to be cancerous (Rauen *et al.*, 2012) and as such are regulated by the Environmental Protection Agency (EPA).

The optimal design of a serpentine baffle tank would involve the addition of the correct number and length of baffles so that the system limits flow separation and dead zones while ensuring that installation and operational costs would be minimized. Money would be wasted in the construction of the tank if too many baffles were added, while the operational cost of the plant would be higher if too few baffles were added. The aim of this chapter is to investigate how internal baffling causes a uniform flow field and minimizes dead volume within the tank. To accomplish this goal, fifty serpentine baffle tank configurations were

modeled using CFD. These tanks all had the same footprint and very similar total detention times. The use of commercial CFD codes in modeling the internal hydraulics of serpentine baffle tanks has already been validated by Amini (2010), Baawain (2006), Falconer (1997), Rauen *et al.* (2008), Taylor (2011), and Zhang (2011, 2012).

3.2 Computational Methodology

The CFD models in the serpentine baffle tank study used the FLUENT methodology outlined in Section 2.4.3. However for the models presented in this chapter the enhanced wall function was not used to handle the near wall turbulence. The standard wall function was used instead as it allowed for meshes with a much smaller total cell size, which allowed for much shorter computational times. The RNG k-ϵ model was used to solve the turbulence closure issue due to its ability to handle flows with both high and low Reynolds numbers (ANSYS, 2011). The Reynolds number of the simulations within the study varied from 2,500 to 10,350 and depended on the number and length baffles within the tank. Each simulation was performed in two steps. First the steady- state solver with a first-order upwind solver was used to converge upon the turbulent steady-state velocity field. Then a passive scalar with a non-dimensional concentration of 1 was injected at the inlet and tracked as it progressed throughout the system using the transient-state solver with a time step of 3 seconds.

3.3 Parametric Baffle Study

3.3.1 Study Methodology

A 1500-gallon tank with a footprint of 11 feet long, 4 feet wide, and 6 feet deep was chosen for the baffle study, as many water providers use a similar style rectangular tank. Figure 3.1a shows the installation of this tank in the Colorado State University (CSU) Engineering

Research Center (ERC) Hydraulics Lab. This type of tank is appealing to many municipalities as a non-pressurized water contact tank due to their large size and relatively low cost. However when these tanks have no internal baffling or inlet modifications, they perform very poorly and are usually credited with a baffle factor of 0.1. The goals of this parametric baffle study are to determine a relationship between the number and length of baffles and the baffle factor, and also the optimal number of baffles.

A similar study was conducted by Taylor (2012) using the footprint of the Embsay contact tank. This current study differs from previous studies due to the inlet configuration used. In the study performed by Taylor (2012), the contact tank was fed water via a rectangular channel. This channel helped to eliminate any internal jets that a pipe feed would induce and significantly improved the tank's efficiency. However this type of inlet configuration is very costly to install and hence more often than not, such rectangular contact tanks have both a round sharp inlet and outlet. Figure 3.1 shows the tank chosen for this study as it was being installed. This tank had three 4-inch outlets on the top and three 2-inch inlets on the bottom of both 4-foot long sides of the tank. This would allow the tank to be easily plumbed in multiple inlet/outlet combinations so that a wide variety of flow conditions could be modeled. Figure 3.1b shows an example of the inlet/outlet conditions that was modeled. It should be noted that the outlet was moved to either side when the placement of baffles dictated that the inlet and outlet could not be placed in line as they are shown in Figure 3.1b. The nondimentional geometric relationships and naming conventions proposed by Taylor (2012) have been adopted in this study to aid the ease of comparison. Taylor (2012) proposed that the optimal baffling could be determined for a tank by one or more of the following relationships: W_{inlet}/W_{ch}, L_T/W_{ch}, L_{bo}/W_{ch}, and L_{bo}/W_{inlet} Taylor (2012). Figure 3.2 shows a plan view of a nine-baffle tank with the geometric naming convention used by Taylor (2012). Taylor (2012) defined W_{ch}, L_{bo}, and L^* using Equations 3.1 to 3.3.

$$W_{ch} = \frac{W_T - \#baffles * W_B}{\#baffles + 1} \tag{3.1}$$

$$L_{bo} = L_T - L_B \tag{3.2}$$

$$L^* = \frac{L_{bo}}{L_T} \tag{3.3}$$

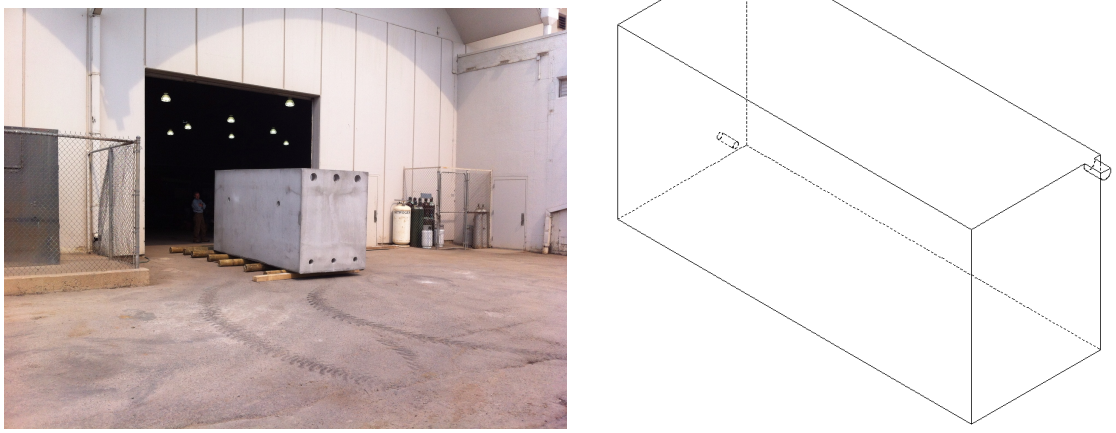

(a) Installation of tank **(b)** FLUENT simulation geometry

Figure 3.1: Tank used in baffle study

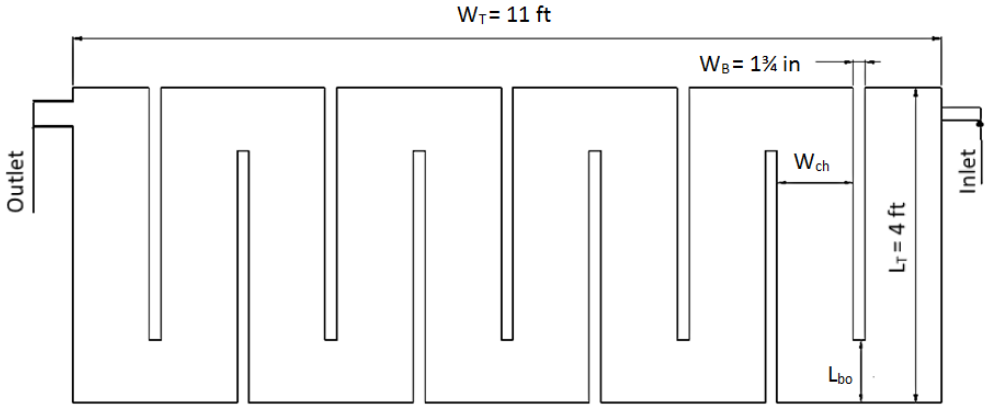

Figure 3.2: Schematic of reference geometries

3.3.2 Additional Study Variables (T_m and R_c/W_{ch})

Two other parameters were also investigated in addition to those proposed by Taylor (2012). These were the dead volume within each tank and a normalized radius of curvature. It was hypothesized that one of these two variables in addition to the geometric design variables proposed by Taylor (2012) would further help explain why certain baffle configurations perform better than others. The dead volume and mean residence time of each simulation was calculated using the formulas outlined by Xu (2010). To determine the dead volume, the mean residence time (T_m) that the tracer spent in the tank for each of the simulations is needed. This mean residence time is calculated as follows:

$$T_m = \int_0^{C_{max}} tdC \approx \sum_{i+1}^{N} (C_i - C_{i-1}) \times T_i \tag{3.4}$$

$$dt = TDT - T_m \tag{3.5}$$

As the tank became more efficient the mean residence time would approach the tank's TDT. The mean residence time could never exceed the tanks TDT due to the formation of jets and eddies which would not occur if the plug flow assumption in the TDT calculation were valid. The difference between the TDT of the tank and the T_m of the tank would yield the contact time lost, dt, from non-plug flow anomalies and can also be equated to the dead volume. By multiplying both the TDT and the T_m by the flow rate of the system, the total tank volume and useful tank volume could be found. Then, the dead volume within the tank was simply the total volume subtracted by the useful volume. It was hypothesized, that as the number of baffles in the tank increased, the dt of the tank would also decrease. After a certain number of baffles had been surpassed, the value of dt would remain constant despite the addition of more baffling. If this happened, then it could have been inferred that the optimal number of baffles had been reached, because adding additional baffles would not

significantly help increase the hydraulic efficiency.

The second parameter that was investigated in addition to those proposed by Taylor (2012) was the normalized radius of curvature (R_c/W_{ch}). This variable was appealing as it could be determined apriori from the geometry of the tank itself. Figure 3.3 shows how the geometric values needed for these calculations were measured as defined by Williams (1986). Figure 3.3a shows the channel parameters as estimated by using only the tank geometry while Figure 3.3b shows the channel derived from the velocity profiles of the tank. It should be noted that for the even baffle configurations the down valley distance, L_{DV}, changed due to different inlet/outlet locations.

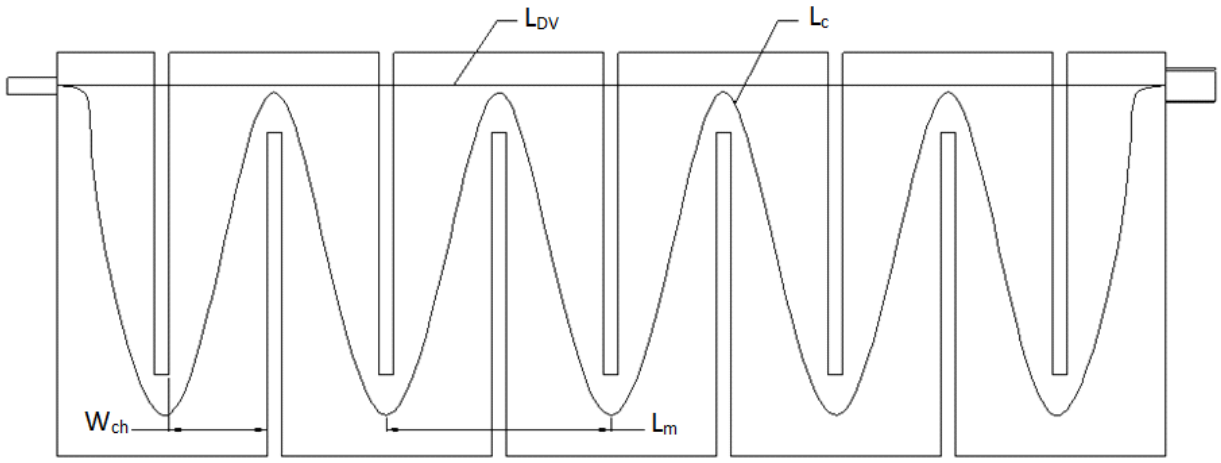

(a) Estimated channel

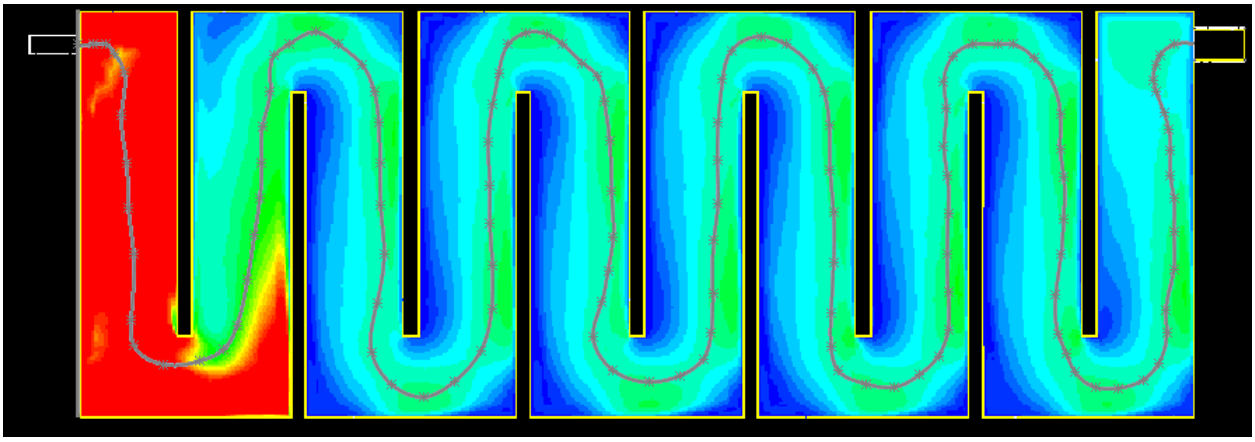

(b) Actual channel from average velocity profiles

Figure 3.3: Calculation of radius of curvature from tank geometry

To calculate the radius of curvature, the wavelength (L_m), channel distance (L_c), down valley distance (L_{DV}), and the channel width (W_{ch}) first had to be measured on each of the simulation geometries. Finally each radius of curvature was normalized by the channel width. In order to verify that the values determined using only the geometry were correct, these same values needed to be determined from the velocity profiles. The simulations that had a L^* of 0.2 were used to validate the values found from the geometry. Once these values had been determined for all 50 simulations the radius of curvature was then calculated for each as follows:

$$K = \frac{L_c}{L_{DV}} \tag{3.6}$$

$$R_c = \frac{L_m K^{1.5}}{13(K-1)^{0.5}} \tag{3.7}$$

3.3.3 Geometry and Meshing

To ensure that the results of the study would be accurate, the simulation geometries and meshes first needed to be created. Since the computational time needed to perform this study using a two-phase model in FLOW-3D would be too costly, a single-phase model was used in FLUENT. However for the single-phase model in FLUENT to be accurate, the flow depth within the tank was first needed. To achieve this the tank shown in Figure 3.1a was recreated in FLOW-3D. A flow rate of 20 GPM was simulated using the methods outlined in Section 2.4.5 up to the introduction of the passive scalar. From this FLOW-3D model it was determined that the fluid depth in the tank for a flow rate of 20 GPM was 5.23 feet.

Using the design parameters outlined by Taylor (2012), a total of fifty simulations were performed with the number of baffles ranging from zero to ten. For each baffle L^* was set to 0.8, 0.6, 0.4, 0.2, and 0.1. With the geometries properly created a parametric study was then performed to determine a mesh with accurate resolution. This parametric mesh study

was performed the same way as the study in Section 2.6.1 with the exception of the standard wall function being utilized and the flow rate had been changed to 20 GPM. None of these meshes used an inflation layer on the walls since the standard wall function in FLUENT would be used. Using the geometry created for the baffleless tank, three different meshes were created. These meshes ranged from 159,551 cells to 916,792 cells. Figure 3.4a shows the maximum velocities from each of the steady-state simulations plotted against the number of cells. This parametric study showed that the mesh containing 337,145 cells would suffice, as this simulation had the highest maximum velocity.

A second parametric mesh study was then performed to determine if the use of the standard wall function would yield accurate results. For this study, the nine-baffle case with an L^* of 0.2 was used to maximize any effects that wall function might have on the results. Figure 3.4b shows the RTD curves produced by the two different wall functions. Since this extreme case only showed a 3% difference in the baffle factor it was decided that the standard wall function would be adequate.

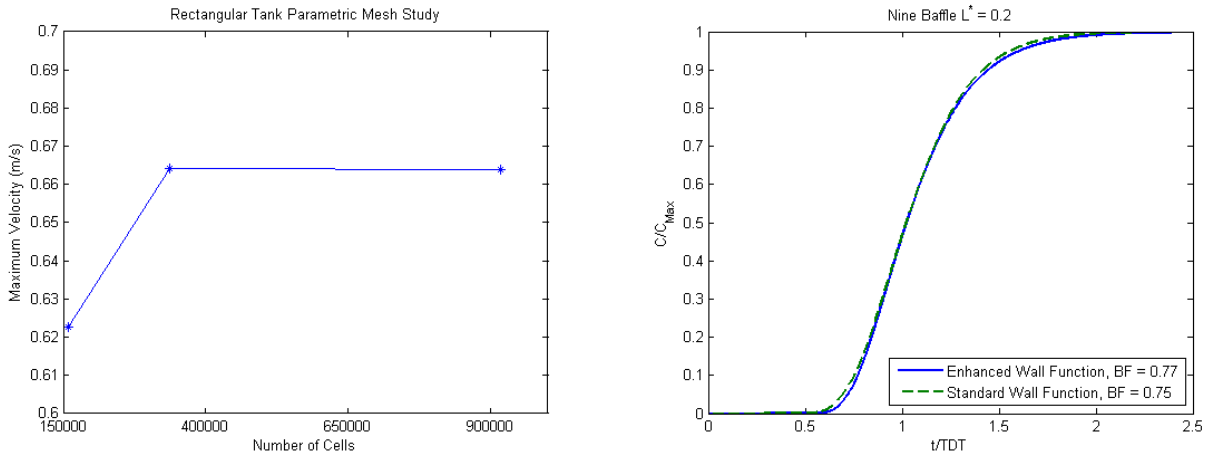

(a) Maximum velocity results

(b) Wall function results

Figure 3.4: Rectangular tank parametric mesh study results

3.4 Baffle Study Results

While this parametric baffle study was in many ways similar to that performed by Taylor (2012), it still yielded new findings. In addition to providing new insight to flow fields within baffled serpentine tanks, this study also verified the ideas put forth by Taylor (2012). Tables 3.1 to 3.5 show the design parameters and results for the 50 simulations within the study. Using only baffles, the baffle factor of the contact tank improved drastically. Without any internal baffling the contact tank had a baffle factor of 0.05, but with the addition of ten baffles this was improved to 0.8. The primary goal of this study was to determine how to better design contact tanks using the non-dimensional parameters discussed in Sections 3.3.1 and 3.3.2.

Figure 3.5 shows the effects of additional baffles on the baffle factor of the system. As this figure shows, there is a clear trend between L^* and the baffle factor of the system. The simulations with an L^* of 20% consistently performed the best, regardless of how many baffles were in the tank. This is in contrast to the results found by Taylor (2012) in which the most efficient L^* varied depending on the number of baffles in the tank Taylor (2012).

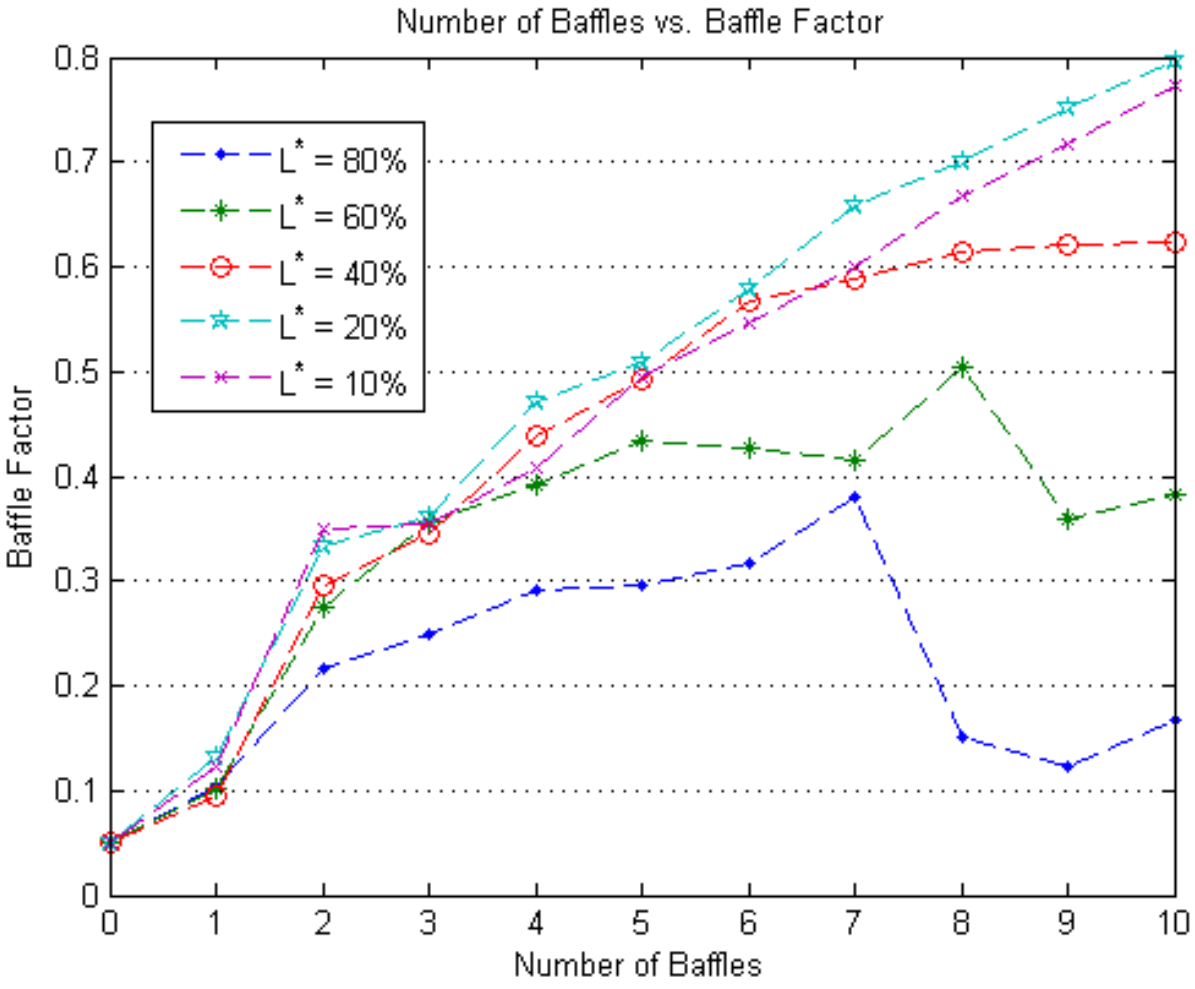

Figure 3.5: Number of baffles vs. *BF*

Table 3.1: Design parameters and efficiencies for $L^* = 0.8$

Number Baffles	Design Parameters				Efficiency					
	W_{inlet}/W_{ch}	L_T/W_{ch}	L_{bo}/W_{ch}	L_{bo}/W_{inlet}	Volume m^3	TDT (s)	BF	T_m	dt	R_c/W_{ch}
1	0.03	0.74	0.59	19.2	6.51	5159	0.11	2932	2226	0.56
2	0.05	1.12	0.90	19.2	6.49	5145	0.22	3216	1928	0.56
3	0.06	1.52	1.21	19.2	6.48	5131	0.25	3356	1775	0.48
4	0.08	1.92	1.54	19.2	6.46	5117	0.29	3525	1592	0.48
5	0.10	2.34	1.87	19.2	6.44	5100	0.30	3697	1402	0.46
6	0.12	2.77	2.21	19.2	6.42	5090	0.32	3487	1602	0.46
7	0.13	3.21	2.57	19.2	6.41	5072	0.38	3741	1330	0.45
8	0.15	3.67	2.93	19.2	6.39	5058	0.15	3106	1951	0.46
9	0.17	4.13	3.31	19.2	6.37	5048	0.12	2898	2150	0.46
10	0.19	4.62	3.70	19.2	6.35	5034	0.17	2845	2188	0.47

Table 3.2: Design parameters and efficiencies for $L^* = 0.6$

Number Baffles	Design Parameters				Efficiency					
	W_{inlet}/W_{ch}	L_T/W_{ch}	L_{bo}/W_{ch}	L_{bo}/W_{inlet}	Volume m^3	TDT (s)	BF	T_m	dt	R_c/W_{ch}
1	0.03	0.74	0.44	14.4	6.49	5145	0.10	2908	2237	0.53
2	0.05	1.12	0.67	14.4	6.46	5117	0.27	3457	1660	0.50
3	0.06	1.52	0.91	14.4	6.42	5090	0.36	3812	1278	0.44
4	0.08	1.92	1.15	14.4	6.39	5062	0.39	3761	1302	0.44
5	0.10	2.34	1.40	14.4	6.35	5030	0.43	3960	1070	0.44
6	0.12	2.77	1.66	14.4	6.32	5006	0.43	4015	991	0.44
7	0.13	3.21	1.93	14.4	6.28	4975	0.41	3908	1067	0.46
8	0.15	3.67	2.20	14.4	6.25	4947	0.50	4092	855	0.47
9	0.17	4.13	2.48	14.4	6.21	4923	0.36	3598	1325	0.50
10	0.19	4.62	2.77	14.4	6.18	4895	0.38	3609	1286	0.51

Table 3.3: Design parameters and efficiencies for $L^* = 0.4$

Number Baffles	Design Parameters				Efficiency					
	W_{inlet}/W_{ch}	L_T/W_{ch}	L_{bo}/W_{ch}	L_{bo}/W_{inlet}	Volume m^3	TDT (s)	BF	T_m	dt	R_c/W_{ch}
1	0.03	0.74	0.29	9.6	6.48	5131	0.10	2892	2239	0.50
2	0.05	1.12	0.45	9.6	6.42	5090	0.30	3512	1578	0.45
3	0.06	1.52	0.61	9.6	6.37	5048	0.35	3790	1258	0.42
4	0.08	1.92	0.77	9.6	6.32	5006	0.44	4019	987	0.43
5	0.10	2.34	0.94	9.6	6.26	4961	0.49	4079	882	0.46
6	0.12	2.77	1.11	9.6	6.21	4923	0.57	4169	754	0.47
7	0.13	3.21	1.28	9.6	6.16	4878	0.59	4198	680	0.51
8	0.15	3.67	1.47	9.6	6.11	4836	0.61	4175	661	0.53
9	0.17	4.13	1.65	9.6	6.05	4798	0.62	4167	631	0.58
10	0.19	4.62	1.85	9.6	6.00	4757	0.62	4130	627	0.60

Table 3.4: Design parameters and efficiencies for $L^* = 0.2$

Number Baffles	Design Parameters				Efficiency					
	W_{inlet}/W_{ch}	L_T/W_{ch}	L_{bo}/W_{ch}	L_{bo}/W_{inlet}	Volume m^3	TDT (s)	BF	T_m	dt	R_c/W_{ch}
1	0.03	0.74	0.15	4.8	6.46	5115	0.13	3110	2005	0.47
2	0.05	1.12	0.22	4.8	6.39	5062	0.33	3670	1392	0.43
3	0.06	1.52	0.30	4.8	6.32	5006	0.36	3849	1157	0.42
4	0.08	1.92	0.38	4.8	6.25	4951	0.47	4113	837	0.44
5	0.10	2.34	0.47	4.8	6.18	4892	0.51	4060	832	0.49
6	0.12	2.77	0.55	4.8	6.11	4840	0.58	4146	694	0.51
7	0.13	3.21	0.64	4.8	6.04	4781	0.66	4209	572	0.57
8	0.15	3.67	0.73	4.8	5.97	4725	0.70	4191	534	0.61
9	0.17	4.13	0.83	4.8	5.90	4673	0.75	4202	471	0.68
10	0.19	4.62	0.92	4.8	5.83	4618	0.80	4188	430	0.71

Table 3.5: Design parameters and efficiencies for $L^* = 0.1$

Number Baffles	Design Parameters				Efficiency					
	W_{inlet}/W_{ch}	L_T/W_{ch}	L_{bo}/W_{ch}	L_{bo}/W_{inlet}	Volume m^3	TDT (s)	BF	T_m	dt	R_c/W_{ch}
1	0.03	0.74	0.07	2.4	6.45	5110	0.12	3195	1915	0.46
2	0.05	1.12	0.11	2.4	6.37	5048	0.35	3904	1144	0.42
3	0.06	1.52	0.15	2.4	6.29	4985	0.36	3884	1101	0.43
4	0.08	1.92	0.19	2.4	6.21	4923	0.41	3958	965	0.45
5	0.10	2.34	0.23	2.4	6.13	4857	0.50	4061	796	0.51
6	0.12	2.77	0.28	2.4	6.05	4798	0.55	4121	677	0.54
7	0.13	3.21	0.32	2.4	5.98	4732	0.60	4168	564	0.61
8	0.15	3.67	0.37	2.4	5.90	4670	0.67	4177	493	0.65
9	0.17	4.13	0.41	2.4	5.82	4611	0.72	4188	423	0.73
10	0.19	4.62	0.46	2.4	5.74	4548	0.77	4170	378	0.77

3.4.1 L^* vs. BF

The discrepancy between L^* results found by Taylor (2012) and those in this study was most likely caused by one of several factors. In the study performed by Taylor (2012), the design variable W_{inlet}/W_{ch} was varied between 0.22 and 1. Due to the small inlet condition that this study used, the W_{inlet}/W_{ch} variable only ranged from 0.03 to 0.19. Since there was no overlap in W_{inlet}/W_{ch} between the two studies, it is possible that the trend in L^* shifts so that it is dependent on the number of baffles in the tank. Another possible reason for the L^* discrepancy could have also been caused by the design variable L_{bo}/W_{inlet}. In the study performed by Taylor (2012), L_{bo}/W_{inlet} ranged from 3.58 to 0.45, while in this study L_{bo}/W_{inlet} was between 19.2 to 2.4. However, since there was an overlap of this variable between both of the studies this is most likely not the primary reason.

The discrepancy in L^* results could have also been caused by the inlet condition itself. While the two tanks in these studies were similar, the inlets were completely different. In the study performed by Taylor (2012), the inlet was located on the side of the tank and was a rectangular channel, while in this study the inlet consisted of a $2''$ pipe located on the bottom front wall of the tank as shown in Figure 3.6. This change in inlet conditions not only allowed the study performed by Taylor (2012) to have different W_{inlet}/W_{ch} and L_{bo}/W_{inlet} values, but also allowed the tank to perform much better without any baffling. This is most evident in the baffle factors between the two tanks without any internal baffling. In the study by Taylor (2012), the case with no baffles had a baffle factor of 0.36 versus the 0.05 of the tank used in this study. After reviewing the data from these two studies it was decided that the size and location of the inlet was the primary factor in the discrepancy between L^* results. The variables W_{inlet}/W_{ch} and L_{bo}/W_{inlet} were not the direct cause of this discrepancy, however a mere by-product of inlet since they both utilized the inlet size in their calculations.

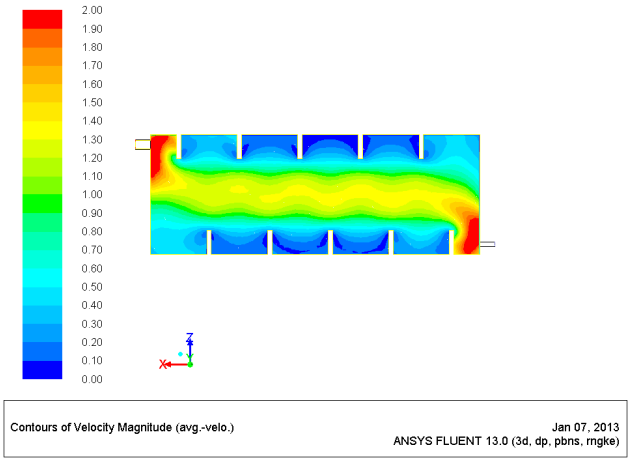

(a) $L^* = 0.8$

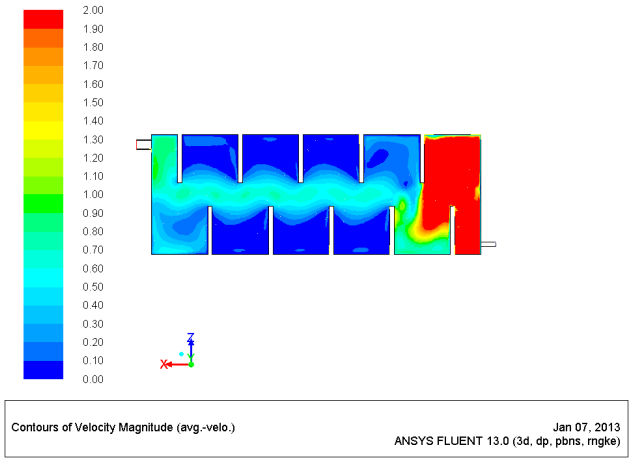

(b) $L^* = 0.6$

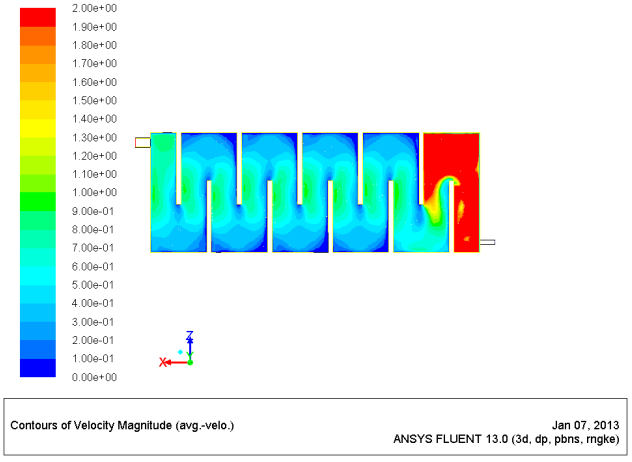

(c) $L^* = 0.4$

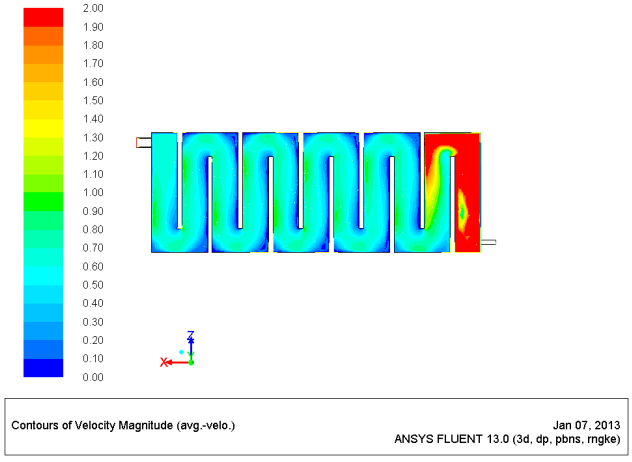

(d) $L^* = 0.2$

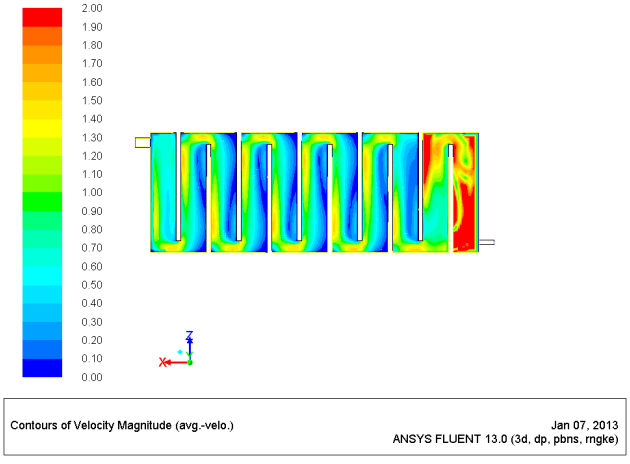

(e) $L^* = 0.1$

Figure 3.6: Mid-depth velocity contours for a 10 baffle tank

Figure 3.6 shows the velocity field for a ten baffle tank with different L^*'s. In each of these simulations the inlet for the tank is on the tank floor in the bottom right corner and the outlet is at the top of the tank in the upper left corner. To highlight the important flow field properties, while maintaining the same color scale for each figure, the plotted velocities shown in Figure 3.6 are a function of the average velocity found in each simulation. As L^* decreases from Figure 3.6a to 3.6e the flow starts to develop a uniform channel with in the tank. Figures 3.6b to 3.6c best show this channeling effect. In Figure 3.6b the flow is mainly along the center of the tank because the baffle tips do not extend past the centerline of the tank. This leads to large dead zones between each of the baffles and a baffle factor of around 0.4.

Once the baffle tips extend past the centerline of the tank as shown in Figure 3.6c the flow is forced around each of the baffles. This extension of L^* by an additional 20% starts to minimize the dead zones within the tank and increases the baffle factor to 0.6. In Figure 3.6d the dead zones have been minimized and the flow has become very uniform. This uniform flow between the baffles is what allows the tank to achieve an optimal baffle factor. Finally Figure 3.6e highlights why an L^* of 0.1 performs worse than that of 0.2. In Figure 3.6e the flow takes on a similar uniform serpentine shape as it did when the $L^* = 0.2$, however the sharp contraction/expansion at the baffle tips creates zones of high velocity. These higher velocity zones cause the tank to deviate from the uniform flow field shown in Figure 3.6d, which in turn causes the baffle factor of the tank to decrease.

Figure 3.7 shows another interesting trend found in this baffle study. The baffle factor of the tank was independent of L^* when only one or two baffles were added. This trend was most likely caused by the alignment and placement of the inlet. Regardless of how long the baffles were, the flow from the inlet would always come into contact with the baffle wall and be dispersed much like in Figure 3.6a. If the inlet was parallel with the baffles instead of perpendicular this trend might not exist. While the one and two-baffle cases were independent of the L^* variable, the two-baffle case always out performed the one-baffle case.

This was caused by the proximity of the first baffle to the inlet. In the two-baffle case the first baffle was much closer to the inlet than the one baffle case. With the first baffle in the two-baffle tank being closer to the inlet, any jet that was formed by the inlet was dispersed sooner. The quick and efficient dispersion of any jets is key to having an efficient tank. Figure 3.6 shows that the jet formed by the inlet conditions is effectively dispersed by the end of the first baffle.

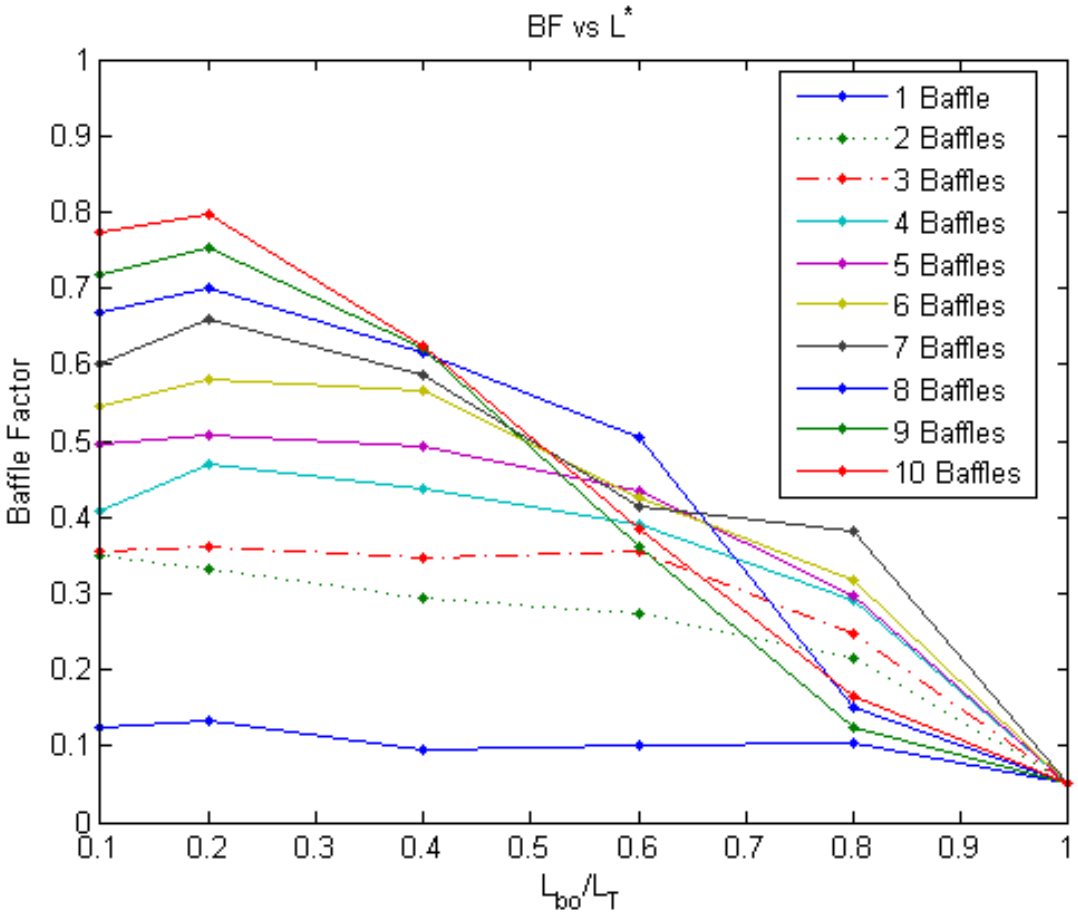

Figure 3.7: *BF* vs. L^*

3.4.2 L_{bo}/W_{ch} vs. *BF*

The design variable of L_{bo}/W_{ch} proposed by Taylor (2012) can be taken as a measure of expansions/contractions within the flow caused by the number and length of baffles. Unlike

the results discussed in the previous section, the trends of L_{bo}/W_{ch} found in this study match well with those found by Taylor (2012). The width of the channel caused by the baffles is equal to the width of the baffle opening when the variable L_{bo}/W_{ch} is equal to 1. When this occurs the baffles are able to maximize the useable volume in the tank by causing a uniform flow field. However, as Figure 3.8 shows, the variable L_{bo}/W_{ch} is not the primary design variable needed to ensure optimum tank efficiency. A prime example of this is the four-baffle case shown as the teal dashed line in Figure 3.8. When there were only four internal baffles in the tank, the baffle factor was highest when the L^* was set to 0.2. With an L^* of 0.2 and four baffles, the L_{bo}/W_{ch} equaled approximately 0.5. The seven-baffle case showed the same trend, with the baffle factor of the tank being highest when L^* equaled 0.2 which yielded a L_{bo}/W_{ch} of 0.63. These two scenarios highlight that the variable L_{bo}/W_{ch} is not the controlling variable governing tank hydraulics. The results of this study indicate that the L^* variable is the most important when designing a baffled contact tank, but it is only a starting point. To have the most efficient baffled tank for a given footprint, this L^* variable should be set to 0.2, then the number of baffles within the tank should be determined by trying to achieve an L_{bo}/W_{ch} close to 1.

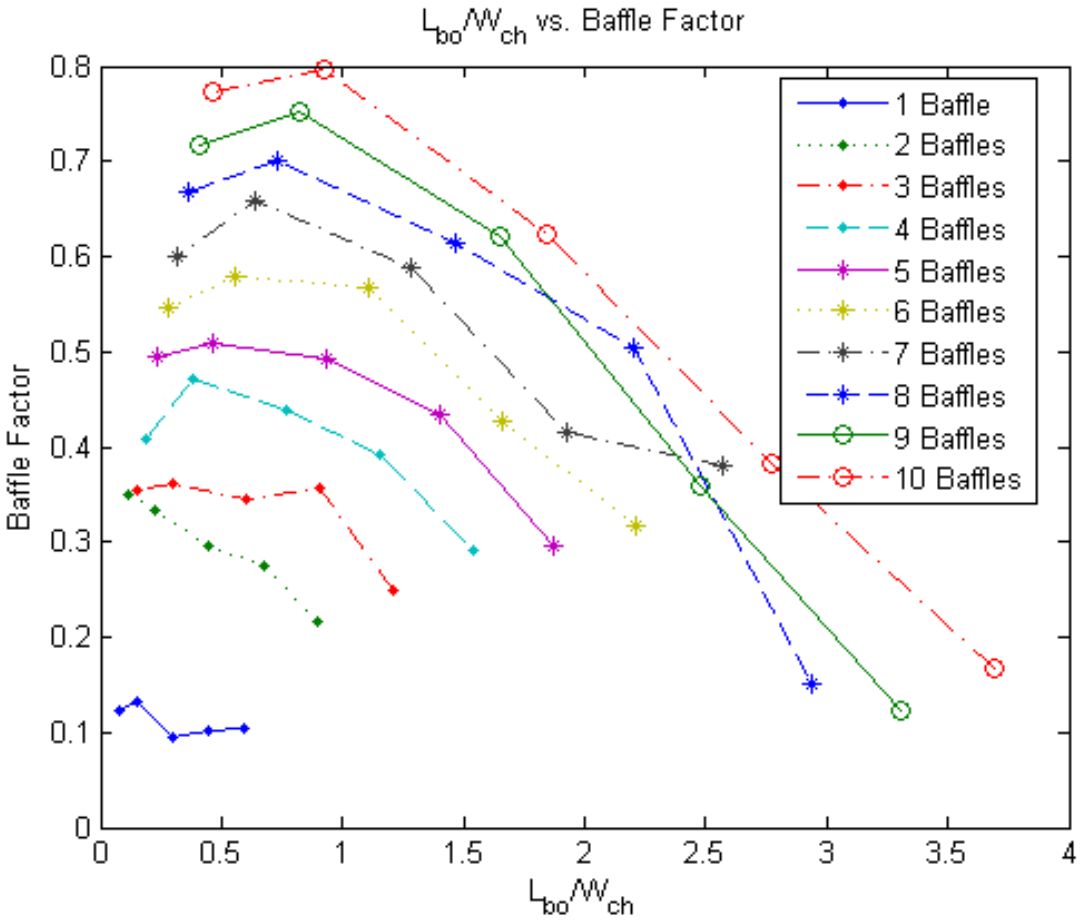

Figure 3.8: L_{bo}/W_{ch} vs. baffle factor

3.4.3 T_m vs. *BF*

While the parameters proposed by Taylor (2012) and investigated in Sections 3.4.1 and 3.4.2 are sound design variables, they do not fully explain the tank hydraulics. To help remedy this, the mean residence time of the tank (T_m) was calculated using the methods outlined in Section 3.3.2. Figure 3.9 shows several plots of T_m for different values of L^*. These figures highlight how the baffles help to channelize the fluid flow. In Figures 3.9a and 3.9b there is no clear trend showing that the baffles are improving the tank hydraulics. This is caused by the short baffling within the tank. Since the baffles do not cross the centerline of the tank the flow simply forms a channel in the middle of the tank, very similar to that seen in Figure

3.6b.

However once the baffle tips cross the centerline of the tank the flow begins to take the serpentine pattern indicative of baffle tanks as shown by Figure 3.9c. In Figure 3.9c the wasted volume represented by dt clearly decreases with the addition of more baffles. Figure 3.9c also shows that there is no significant gain in tank efficiency after seven baffles when L^* is set to 40%. Figures 3.9d and 3.9e show similar results however raise some interesting points. In Figure 3.9d it seems that the optimal number of baffles is between 9 or 10 as the dt value begins to plateau. However in Figure 3.9e the dt value is still steadily decreasing, which indicates that the optimal number of baffles for an L^* of 10% has not yet been reached. Figure 3.9d is in agreement with the results discussed in Sections 3.4.1 and 3.4.2. Using the results from these three sections it appears that ten baffles would be the optimum number for this contact tank. Placing more than ten baffles within this tank would yield a higher baffle factor, but with a lower return for additional baffles.

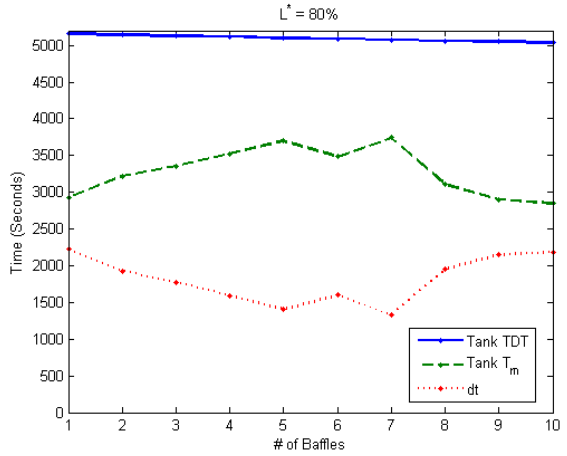

(a) $L^* = 0.8$

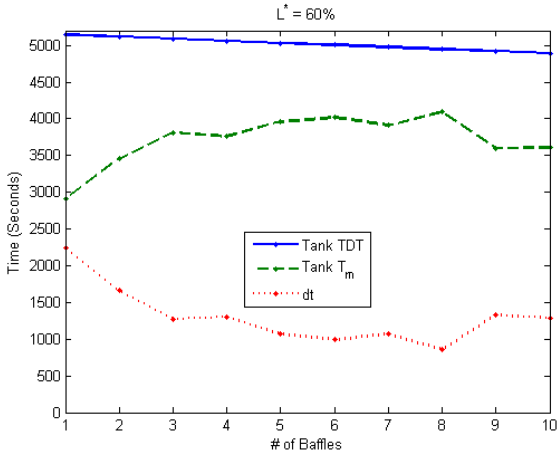

(b) $L^* = 0.6$

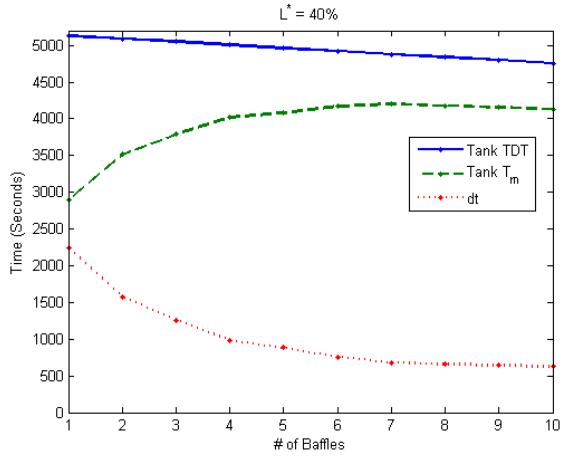

(c) $L^* = 0.4$

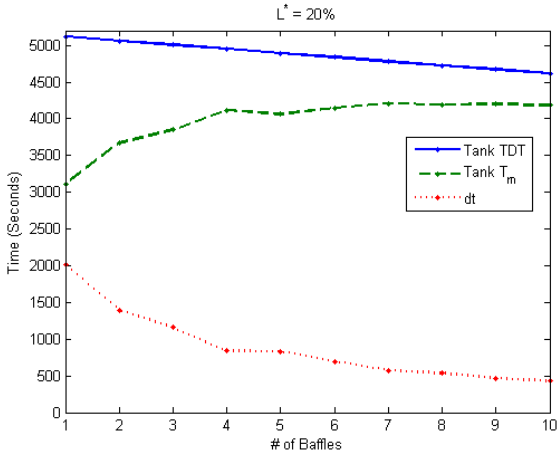

(d) $L^* = 0.2$

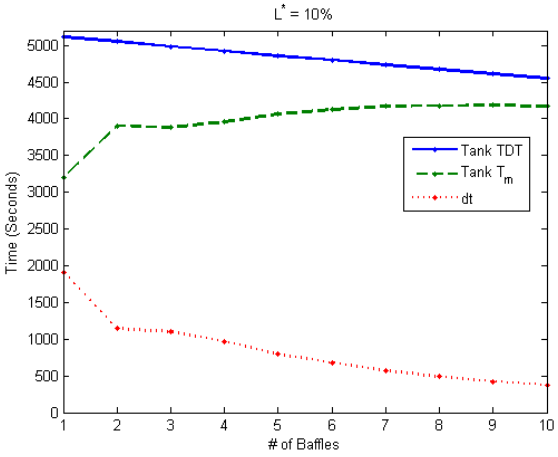

(e) $L^* = 0.1$

Figure 3.9: T_m vs. number of baffles for various L^*'s

3.4.4 R_c/W_{ch} vs. BF

The normalized radius of curvature (R_c/W_{ch}) has traditionally been a variable used to describe the meanders of rivers. According to Williams (1986), the variable R_c/W_{ch} is important in river mechanics as numerous hypotheses use it to identify trends in: flow resistance and bend migration rates; separation-collapse theory; and flow-momentum bank erosion models. Since the cross sectional velocity profile shown in Figure 3.6d very closely resembles that of a meandering river, it was hypothesized that the R_c/W_{ch} variable might also yield some new insights into serpentine baffle tanks. Figure 3.10 shows the R_c/W_{ch} values calculated from each of the simulations for the five different values of L^*. Much like the results of T_m found in the previous section, there is no trend between R_c/W_{ch} and the baffle factor if L^* was less than 40% as shown in Figures 3.10a and 3.10b.

An interesting trend in Figures 3.10c to 3.10e was that R_c/W_{ch} and the baffle factor did not match up until there were at least four baffles within the tank. However these figures do show that the variable R_c/W_{ch} does seem yield results that are very similar to the baffle factor of the tank. Figure 3.10d also shows the R_c/W_{ch} values that were calculated from the cross sectional velocity profiles found in FLUENT with those measured from the tank geometry. This figure shows there is good agreement between the R_c/W_{ch} values estimated from the tank geometry with those measured from the velocity profiles. It is of interest that the variable R_c/W_{ch} was accurately calculated from the tank geometry despite the differences in measurements as shown in Figure 3.3.

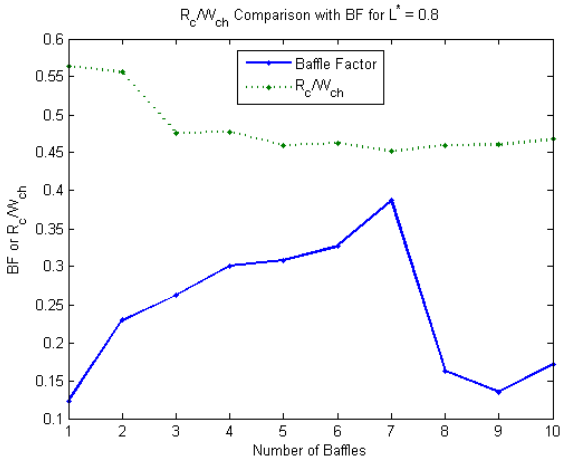

(a) $L^* = 0.8$

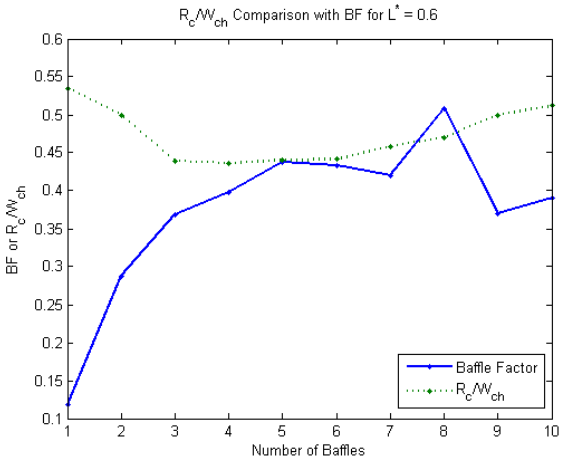

(b) $L^* = 0.6$

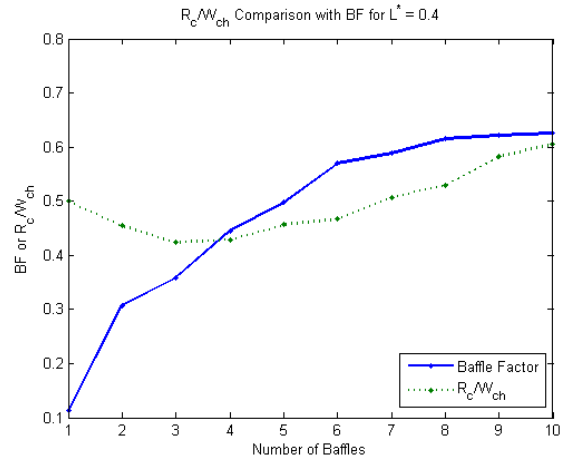

(c) $L^* = 0.4$

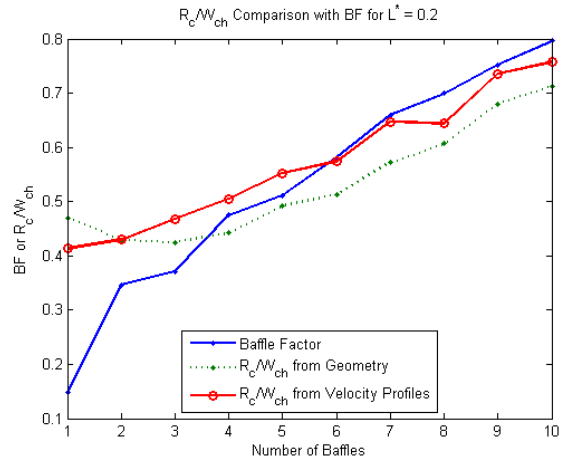

(d) $L^* = 0.2$

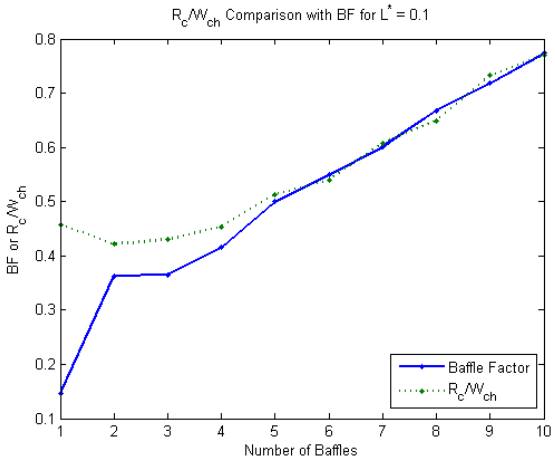

(e) $L^* = 0.1$

Figure 3.10: R_c/W_{ch} vs. number of baffles for various L^*'s

3.5 Conclusions

The results presented in this chapter show that the addition of internal baffling can greatly improve the hydraulic efficiency of a rectangular contact tank. These baffles create a uniform flow field within the contact tank if they are properly designed. From the results of this study the baffle opening ratio L^* should be set between 0.1-0.2. Then the number and placement of baffles within the contact tank should be determined by trying to achieve a L_{bo}/W_{ch} ratio close to 1 as discussed in Section 3.4.2.

While the variables T_m and R_c/W_{ch} provided an interesting insight to the flow field, their use in designing tanks is limited. The primary issue with T_m is that it cannot be determined apriori. T_m can only be calculated once a physical tracer study or a CFD analysis has been performed using the contact tank. R_c/W_{ch} initially looked promising as it could be determined apriori, however more research needs to be conducted before its use can be validated. Specifically this variable needs to be used on tanks that have baffles oriented 90° to those used in this study.

Additional CFD models and physical tracer studies are needed to fully validate all of the results in this chapter. The rectangular concrete tank installed in the CSU ERC Hydraulics Lab will be used for this purpose. This tank will have internal baffles added to validate the results presented in this chapter. The following chapter presents a cases study of a serpentine baffle tank in Jamestown, Colorado.

Chapter 4

Jamestown Case Study

4.1 Introduction

While computational modeling and lab experiments are very useful, their suitability for real world applications needs to be addressed. To help bridge the gap between laboratory studies and prototype systems, an existing physical system was needed. The Colorado Department of Public Health and Environment (CDPHE) decided that the water treatment system operated by the city of Jamestown, Colorado would be an ideal candidate for this. The system in Jamestown had a history of water quality issues and due to the small size of the town, they also had insufficient funds to improve the system themselves. The Jamestown Case Study consisted of three phases: 1) initial site visit/ define project goals; 2) CFD modeling and tracer studies of the existing system; 3) CFD modeling, installation, and tracer studies of system modifications.

4.2 Computational Methodology

The set up of the CFD simulations performed on the Jamestown chlorine contact tank were very similar to those described in Chapter 3. However, some of the simulations performed in this chapter utilize the laminar flow model in ANSYS FLUENT. This model was used when the Reynolds Number of the flow deemed it necessary. All of the turbulent simulations used the k-ϵ RNG model with an enhanced wall function. Each simulation was allowed to reach a steady-state solution before a transient time scheme was implemented. After the steady-state velocity field had been calculated a passive scalar was introduced at the inlet

and tracked as it progressed throughout the tank in time.

4.3 Phase 1: Initial Site Visit and Project Goals

During the initial site visit, the two water treatment plant operators gave a tour of the facility and expressed their goals for the outcome of the study. The treatment plant in Jamestown was built in the early 1990's and consisted of two slow sand filters that fed into a long serpentine baffle tank shown in Figure 4.1. At the time of the case study, Jamestown was one of only a handful of drinking water treatment plants that used a slow sand filter in Colorado.

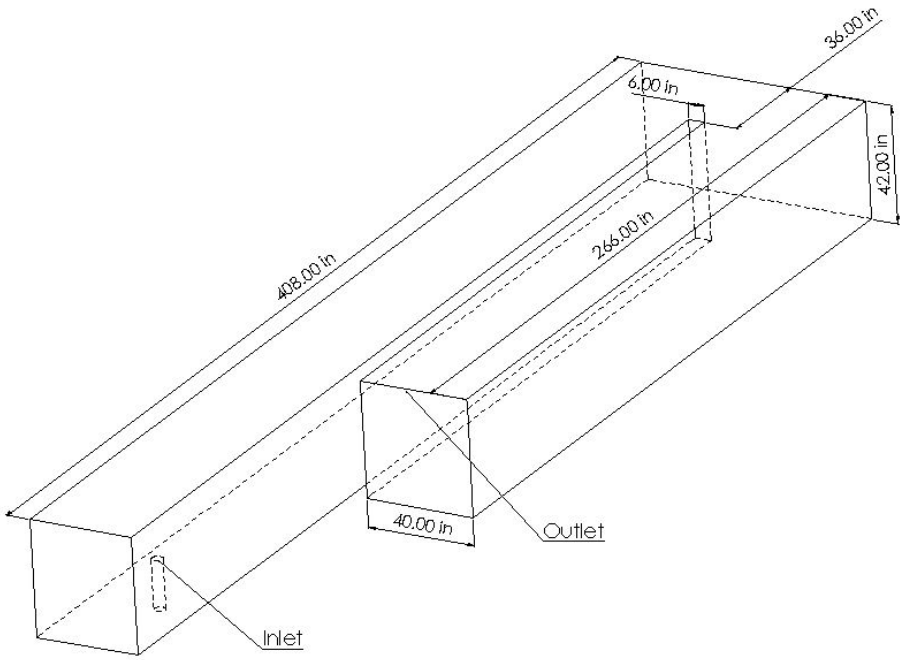

Figure 4.1: Geometry of the Jamestown contact tank

During the initial meeting, the plant operators said that the original design flow rate of the plant was 180,000 GPD and that the typical operational flow rates for the plant were around 80,000 GPD in summer and 20,000 GPD in the winter. The plant operators also stated that one of the primary issues of the plant was that the efficiency of the tank

decreased during the low flow winter months. This issue was peculiar as contact tanks tend to perform better under lower flow rates than at higher flow rates. It was hypothesized by the researchers that during the low flow months, the flow within the contact tank was changing from a turbulent to laminar flow regime. With this issue in mind, the plant operators stated that from this project they wanted to know the baffle factors of the contact tank under their normal operating flow rates and that the difference between the high flow and low flow BF's be no more than 10%.

4.4 Phase 2

Using blueprints of the contact tank that were provided by the plant operators, a three-dimensional computer model of the existing tank was constructed. Since the outlet of the tank was a sharp crested weir, the flow depth over the weir was determined for the two flow rates by:

$$Q = \frac{2}{3} C_d b \sqrt{2g} h_1^{\frac{3}{2}}$$

Where:

$$Q = inflow\ rate\ in\ \frac{m^3}{s}$$

$$C_d \approx 0.611$$

$$b = tank\ width = 0.97m$$

$$g = gravity = 9.81 \frac{m}{s^2}$$

$$h_1 = flow\ depth\ over\ weir\ in\ m$$

Then h_1 was solved iteratively using the solver function in Microsoft Excel. The results for the flow depth over the weir are shown in Table 4.1.

Table 4.1: Flow depths over the outlet weir.

Flow Rate (GPD)	Flow Depth (m)	Flow Depth (in)
20,000	0.025	0.98
80,000	0.063	2.47

4.4.1 CFD Modeling

With the geometry properly created, a parametric study was performed to determine the mesh size needed to properly resolve the flow field. It was decided that the 20,000 GPD flow rate would be used for these studies. A total of four different meshes were constructed that encompassed a wide range of total cells as shown in Table 4.2.

Table 4.2: Summary of the meshes used in parametric study

Mesh Name	Total Cells
Fine	304,605
Medium with Inflation Layer	166,853
Medium	67,313
Coarse	79,304

In all of the parametric studies, expect the medium with inflation layer, the k-ϵ RNG model with standard wall functions was used to resolve the turbulence. In the medium with inflation layer the k-ϵ RNG model with an enhanced wall function was used. All these models were first allowed to run until a steady-state solution was found before a transient time scheme was used to track a passive scalar through the system. Figure 4.2a shows the RTD curves and baffle factors for each of these simulations. After examining Figure 4.2a it became apparent that the baffle factor and RTD curves alone would not be an accurate way of determine which mesh to use. All of the RTD curves were very similar and had comparable baffle factors, so another indicator was needed to determine the optimum mesh. To remedy this, the maximum velocities found in each simulation were plotted against the

total number of cells in each mesh as shown in Figure 4.2b. This figure shows that the grid resolution was sufficient to accurately model the flow field as there was very little variation in maximum velocities between simulations. Since all the meshes yielded similar results, the medium resolution mesh with an inflation layer was used for the rest of the parametric studies. This mesh was chosen because it had a higher resolution near the walls of the tank and would allow for the use of the enhanced wall function in FLUENT.

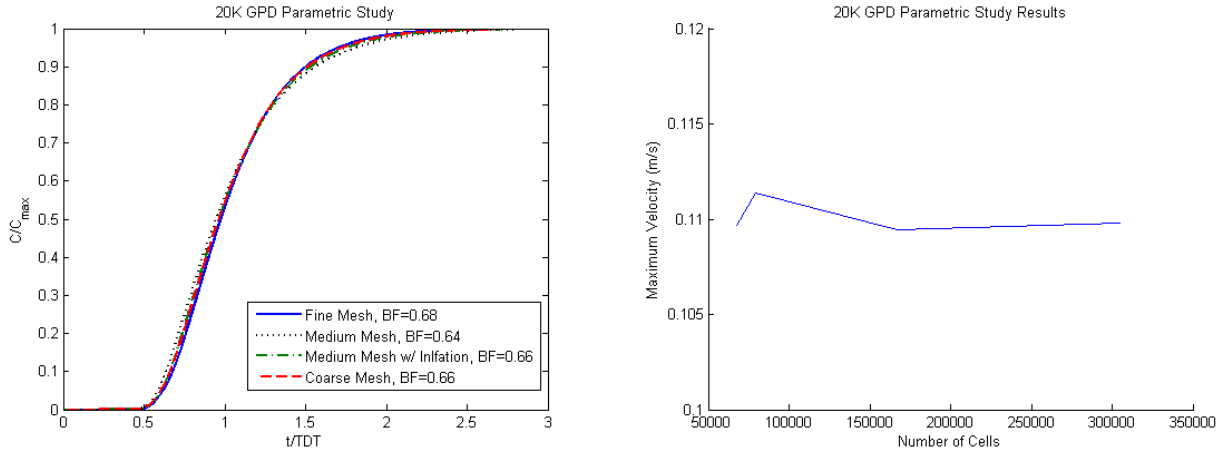

(a) RTD curves for the parametric study

(b) Maximum velocity results

Figure 4.2: Results of the 20,000 GPD parametric study

With the mesh properly sized so that the flow field was accurately resolved, attention was then turned to the flow regime during the 20,000 GPD flow rates. To determine if the flow was laminar or turbulent the average velocity magnitude of the medium mesh with inflation layer was needed to calculate the Reynolds Number. Using the volume reports feature in FLUENT, the average velocity magnitude was found to be 0.00158 m/s. Since the flow depth and width were known from the geometry of the tank, the Reynolds Number was calculated as:

$$H_d = Hydraulic\ Diameter = \frac{4WH}{W+2H} = \frac{4 \times 0.97m \times 1.07m}{0.97m + 2 \times 1.07m} = 1.33m$$

$$Re = \frac{\rho H_d V_{avg}}{\mu} = \frac{998.2\frac{kg}{m^3} \times 1.33m \times 0.00158\frac{m}{s}}{0.001003\frac{Ns}{m^2}} = 2,089.0$$

For conduit flow the flow regime is laminar if the Reynolds Number is less than 2,300 and turbulent if the Reynolds number is greater than 4,000. Since the Reynolds Number of the flow from the turbulent model was 2,089, the results of this model were incorrect. This simulation was then rerun with a laminar model instead of the turbulent k-ϵ RNG model. With the turbulence model turned off, the average velocity magnitude was 0.00197 m/s which produced a Reynolds Number of 2,608. Since this number is slightly larger than 2,300 the flow can be classified as a transitional flow regime. In a transitional flow regime the flow can either be laminar or turbulent depending upon the roughness of the walls and the uniformity of the flow. A tracer study was conducted to validate that the flow regime was indeed laminar and is shown in Figure 4.3. In all of the following, simulations with a flow rate of 20,000 GPD were modeled as laminar. Figures 4.3 and 4.4 show the RTD curves with the baffle factors for the existing system in Jamestown. These results showed that the baffle factor of this system varied between 0.52 and 0.63.

4.4.2 Tracer Studies

Tracer studies were then performed on the existing system so the computer models could be validated. These tracer studies were conducted by injecting a solution of Lithium Chloride into the influent and then samples were collected at the weir. The tracer solution was injected into the influent via a secondary chlorine injection port that was located just upstream of the primary chlorine injection port. This secondary port was no longer used and allowed the tracer study to be conducted while the plant was still operational. Due to the small size of the plant, most of the chlorine contact tank was located under the plant office. A floor covered the remaining section of the contact tank so that the service pumps could be housed inside of the building. An access port in the floor, which was within arms reach of the weir, was discovered and used to take effluent samples. The Lithium Chloride solution was mixed

so that the effluent concentration would not exceed 0.04 mg/l. While the tracer studies were being performed, an anomaly was noticed within the tank that was not accounted for within the CFD simulations.

During the operation of the contact tank the treated effluent spilled over the weir into a collection tank before being pumped into the supply system. This collection tank had two service pumps, which were activated by a float switch, however this float switch would not engage until the weir had been completely submerged. While the weir was submerged the water in the collection tank with a lower tracer concentration was allowed to mix with the water upstream of the weir with a higher concentration. This mixing diluted the upstream tracer concentration, which is evident in Figures 4.3 and 4.4. In Figures 4.3 and 4.4 the points marked by ⓧ were those that were taken when the weir was completely submerged. From the CFD and tracer results, the baffle factor of the system varied between 0.5 and 0.6.

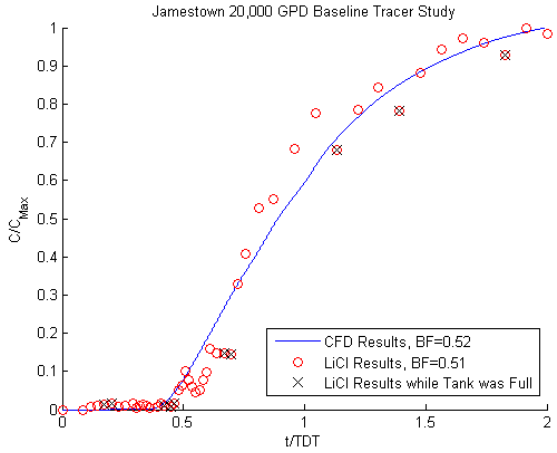

Figure 4.3: Tracer results for 20,000 GPD

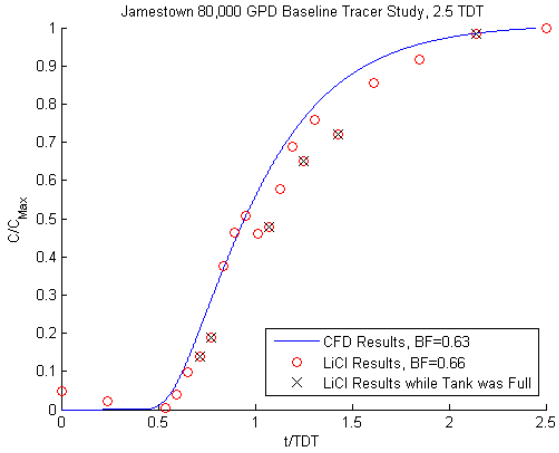

Figure 4.4: Tracer results for 80,000 GPD

4.4.3 Phase 2 Results

The CFD models coupled with the tracer studies proved that the suspicion of the plant operators was correct. During the low flows, the BF of the contact tank dropped by over 17%. This decrease was caused by the change in flow regimes from turbulent to laminar.

To further investigate this matter cross sectional velocity profiles were developed from the CFD model to compare the two different flow regimes. Figure 4.5 shows where these cross-sectional profiles were taken from, although only a few stations will be presented to avoid repetition. Figures 4.6 to 4.8 show the cross sectional velocity profiles at their respective stations. In each of these figures, the velocity has been normalized by the respective average velocity of the entire tank. It should be noted that the velocity profiles near the wall in these figures are slightly incorrect. The fluctuations in the near wall velocity arose from how MATLAB processed the information that was exported from FLUENT. These fluctuations are not found in the simulation and are simply a graphical plotting error in MATLAB.

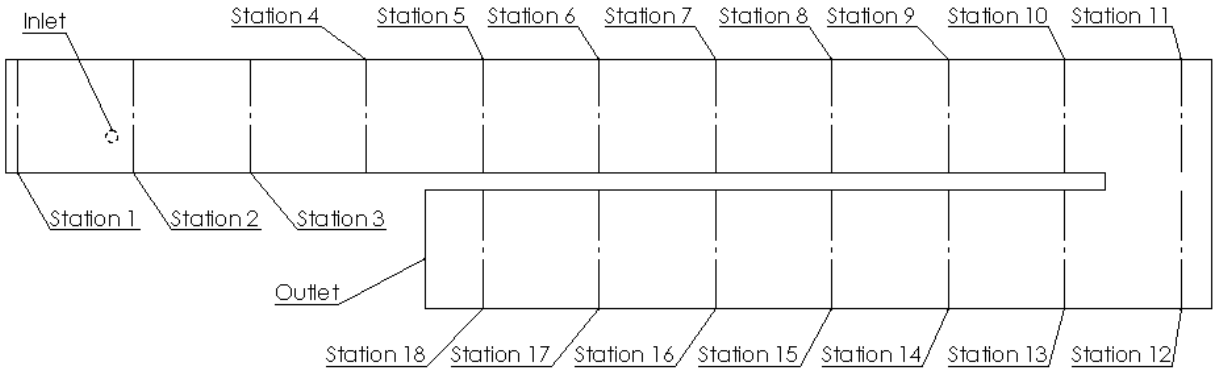

Figure 4.5: Location of stations within the tank where velocity profiles were obtained

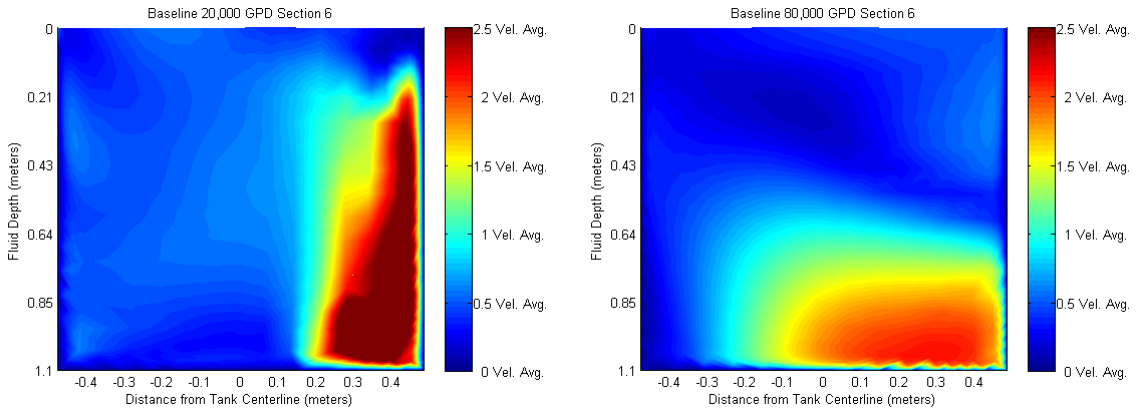

(a) 20,000 GPD **(b)** 80,000 GPD

Figure 4.6: Velocity profiles at section 6

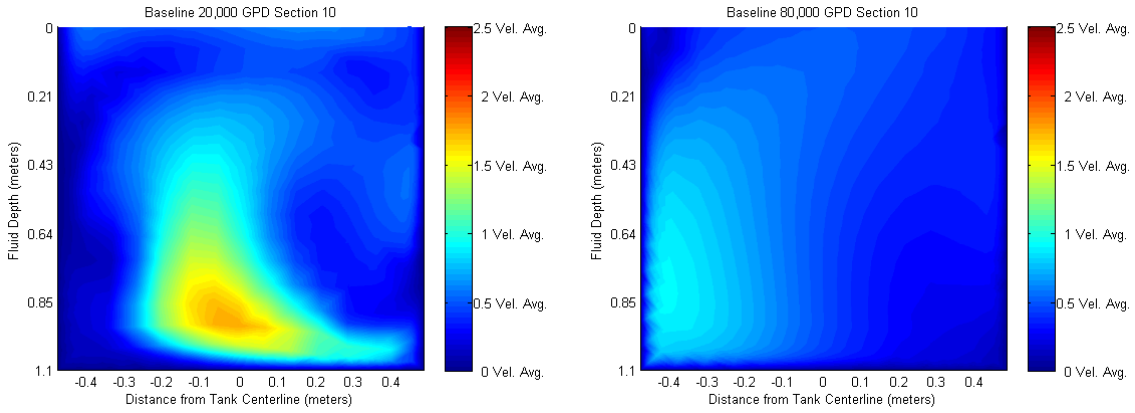

(a) 20,000 GPD **(b)** 80,000 GPD

Figure 4.7: Velocity profiles at section 10

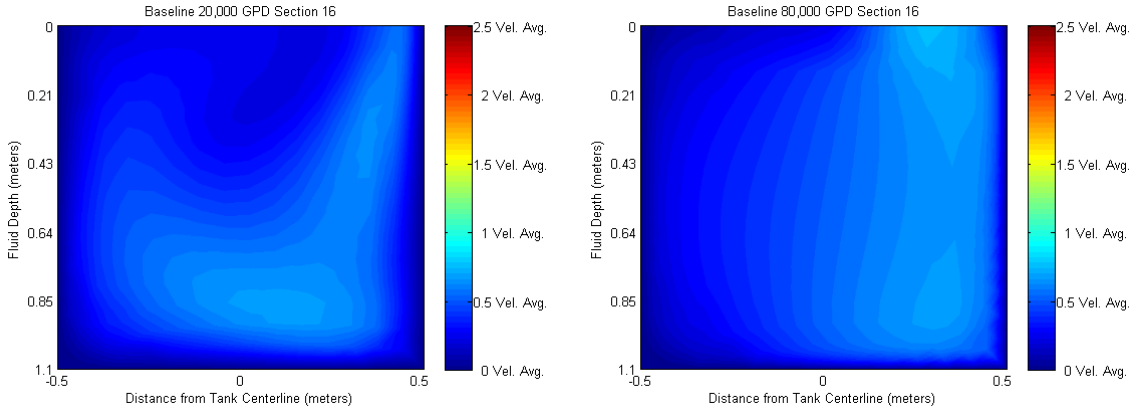

(a) 20,000 GPD **(b)** 80,000 GPD

Figure 4.8: Velocity profiles at section 16

Figure 4.6 shows that a jet forms within the tank downstream of the inlet at both flow rates. This jet begins to disperse at the higher flow rate as shown in Figure 4.7b. Figure 4.8 shows the cross-sectional velocity profile at Station 16. As this figure shows, the flow has become relatively uniform, although the higher flow rate in Figure 4.8b shows that the velocity is more uniform than that of the lower flow rate. The jet that occurs at the lower flow rate as shown in Figures 4.6a and 4.7a causes a significant loss of tank volume. This jet disappears much faster in the higher flow rate because the turbulence within the flow is

able to dissipate the jet by mixing as shown in Figures 4.6b and 4.7b. Figures 4.9 and 4.10 show horizontal velocity profiles of the tank at different elevations. These two figures clearly show the internal jet and how it is dissipated much earlier in a turbulent flow.

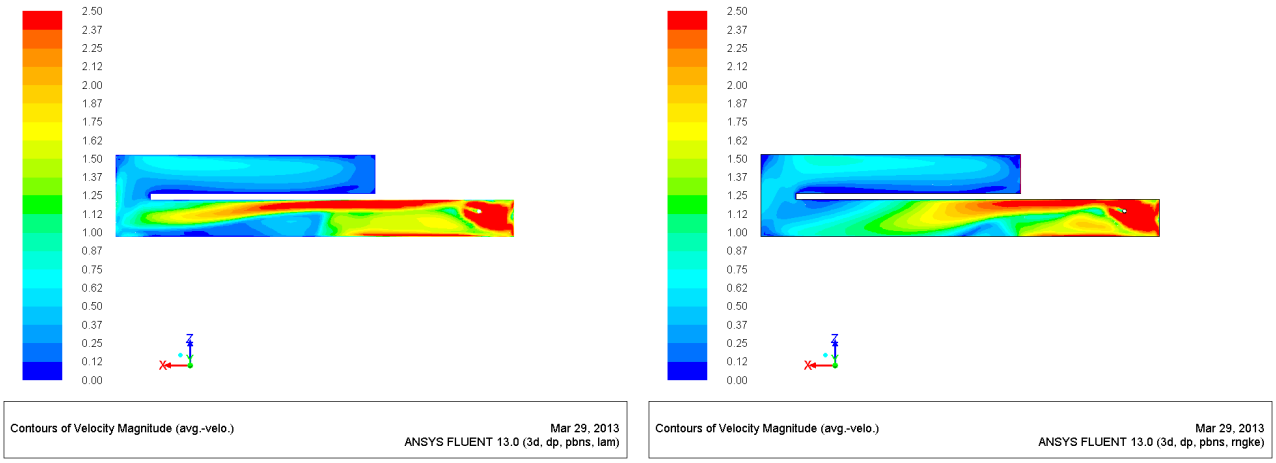

(a) 20,000 GPD **(b)** 80,000 GPD

Figure 4.9: Velocity profile 0.1 meters off of tank bottom

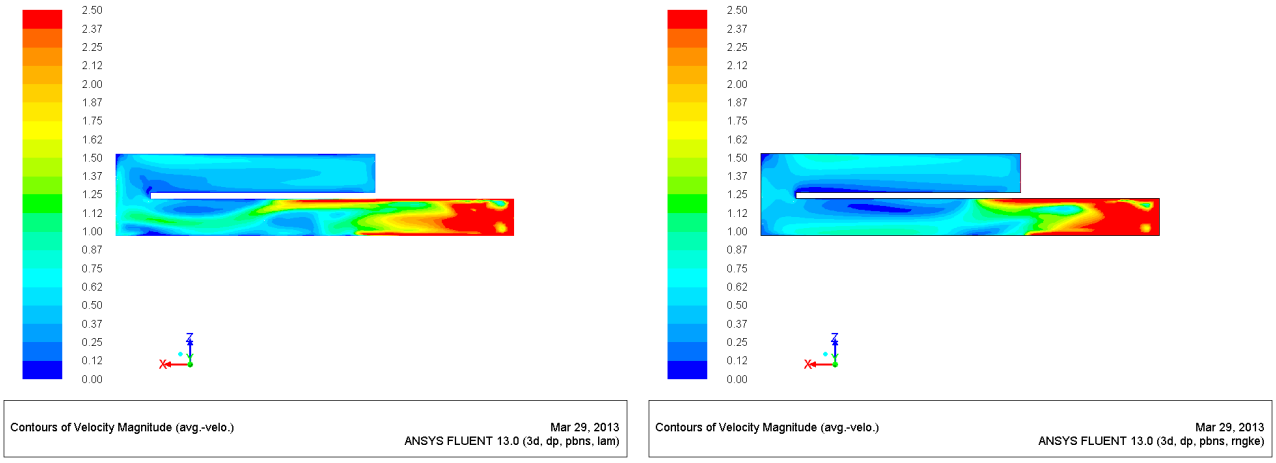

(a) 20,000 GPD **(b)** 80,000 GPD

Figure 4.10: Velocity profile 0.5 meters off of tank bottom

While the cross-sectional velocity profiles shown in Figure 4.8 are relatively uniform, their velocities are much slower than the average. Since the existing inlet does little to reduce the influent velocity, and in effect the influent energy, there are large areas near the inlet that

have velocities up to 55 times higher than the average. These figures along with Figures 4.9a and 4.10a prove that the tank was well designed but the inlet was not. In all of these figures, the internal jet caused by the inlet design has either dissipated or is in the process of dissipating. If the inlet was properly designed the areas shaded red (i.e. having a velocity greater than 2.5 times the average) would be minimized while the green areas (i.e. having a velocity between 0.8 to 1.4 times the average) would be maximized.

The design of the Jamestown contact tank was also investigated using the dimensionless relationships outlined in Chapter 3. Since the channel widths (W_{ch}) varied along with the channel lengths (L_T) it was difficult to determine the exact design variables as laid out in Chapter 3. Despite this it was found that L^* varied between 0.10 and 0.16 while L_{bo}/W_{ch} was between 0.90 and 0.95. These two values are within the range that Chapter 3 found for the tank to be optimal. However, since the baffling in the Jamestown tank was oriented 90° perpendicular to those used that study in Chapter 3, the variable R_c/W_{ch} was not close to the BF and was instead around 14.8 to 15.5.

4.5 Phase 3

4.5.1 CFD Modeling

Since Jamestown did not have sufficient funds for a major redesign of the contact tank, it was decided that only modifications to the inlet would be investigated. Previous investigations of inlet modifications have shown that they are most effective when the modification causes a uniform flow field and dissipates energy in the flow Taylor (2012). This dissipation of energy helps to discourage the formation of internal jets, similar to those seen in Section 4.4. With this in mind, an idealized inlet condition was first modeled with the goal of determining the maximum baffle factor that the system could achieve with only inlet modifications. Figure 4.11 shows the tank geometry for this case. In this configuration, the entire front wall of the

tank was used as an inlet so the flow could be as uniform as possible. From these simulations it was determined that the baffle factors could theoretically go as high as 0.67 for the 20,000 GPD case and 0.75 for the 80,000 GPD case using only inlet modifications.

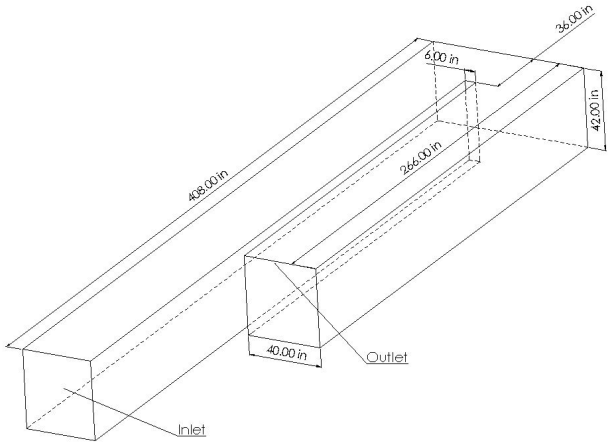

Figure 4.11: Tank geometry for the best-case inlet

The first proposed modification used a 90° elbow on top of the inlet to redirect the flow toward the front wall as shown in Figure 4.12. The second modification involved placing a tee on top of the inlet to split the flow in two with 90° elbows placed on either end of the tee to direct the flow towards the front wall like the previous modification (see Figure 4.13). Both modifications involved pointing the influent toward the front wall in order to use this wall to dissipate energy from the flow. With the inlets facing this front wall, it was expected that the flow would spread out and mimic the idealized case after hitting the wall. The front wall of the tank would also discourage the formation of the downstream jet by dissipating energy from the influent. To simplify the two-inlet cases, it was assumed that the flow would be equal out of both the inlets. Table 4.3 shows the results of a parametric study performed on inlet structure for this modification. As this table shows, assuming an equal flow rate through both inlets is appropriate.

Figures 4.14 and 4.15 show the envelopes of the RTD curves for both of the flow rates along with how the inlet modifications could improve the system efficiency. Figure 4.14 shows just how much the proposed modifications could improve the system at the 20,000

Table 4.3: Inlet flow rates for the tee inlet manifold

	Percentage of Total Flow	
	20,000 GPD	80,000 GPD
Left Inlet	49.9%	51.9%
Right Inlet	50.1%	48.1%

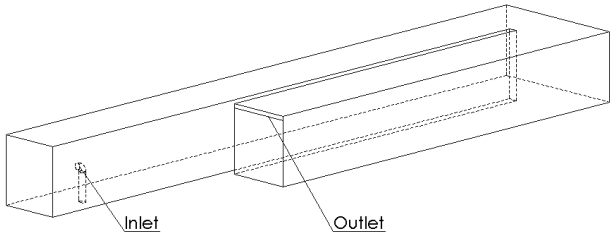

Figure 4.12: 90° elbow geometry

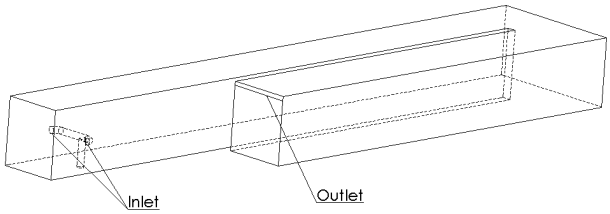

Figure 4.13: Tee geometry

GPD flow rate. The RTD curves for the two-inlet tee modification almost matches that of the idealized best-case scenario. Figure 4.15 shows the same RTD curve envelope for the 80,000 GPD cases. This figure clearly highlights that the proposed inlet modifications would have very little effect on the higher flow rate. From these RTD curves, it was decided that the two-inlet tee modification would be proposed to the plant as the best option.

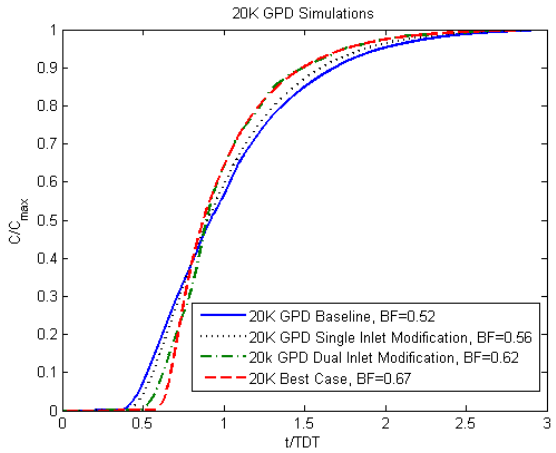

Figure 4.14: RTD curves for the 20,000 GPD simulations

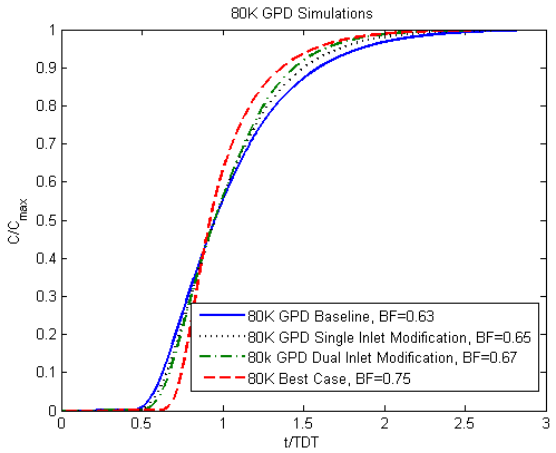

Figure 4.15: RTD curves for the 80,000 GPD simulations

Figures 4.16 to 4.18 show the cross sectional velocity profiles created by the split tee

modification and are taken at the same locations as those shown in Section 4.4. These figures show a flow field that is much more uniform than the existing flow fields found in Figures 4.6 to 4.8.

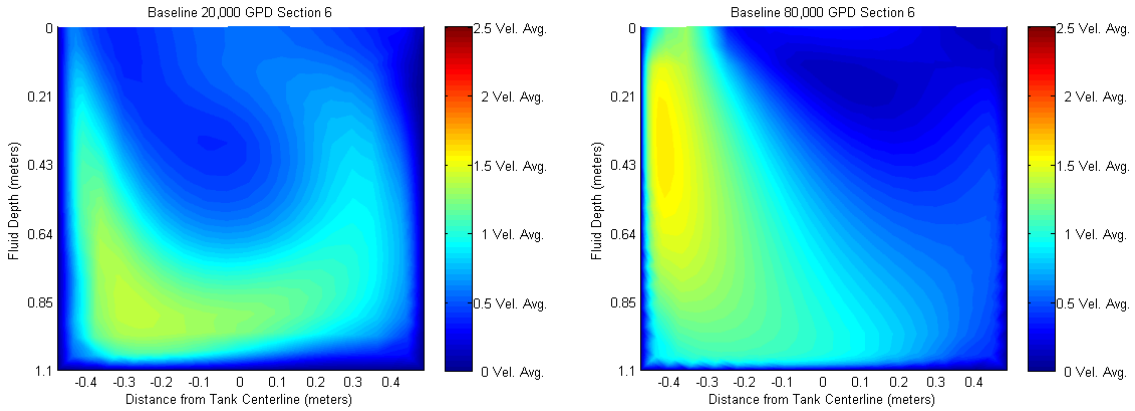

(a) 20,000 GPD **(b)** 80,000 GPD

Figure 4.16: Velocity profiles at section 6 for the tee inlet

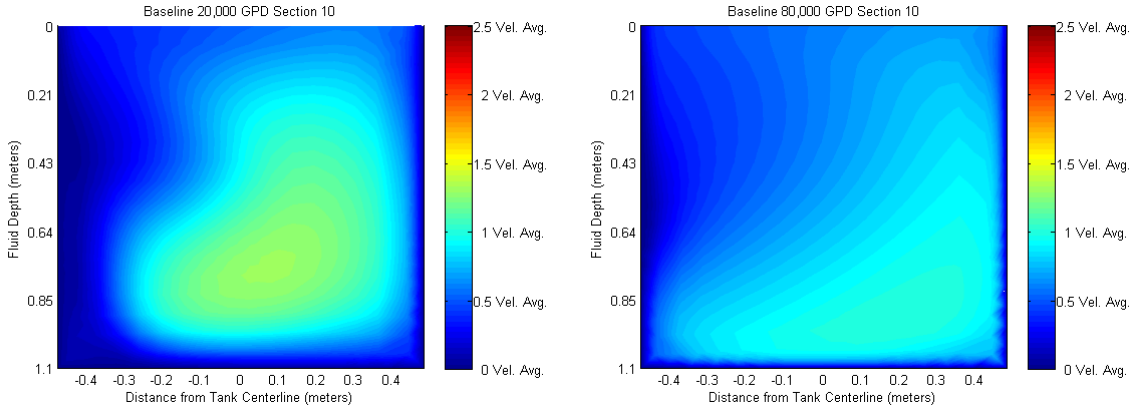

(a) 20,000 GPD **(b)** 80,000 GPD

Figure 4.17: Velocity profiles at section 10 for the tee inlet

Figures 4.19 and 4.20 also show a significant reduction in areas were the velocity is higher than 2.5 times the average from the baseline case. These various cross sections show that tee inlet modification could influence the velocity fields in a favorable manner as needed. This inlet manifold was designed in such a way that it would: dissipate energy from the flow;

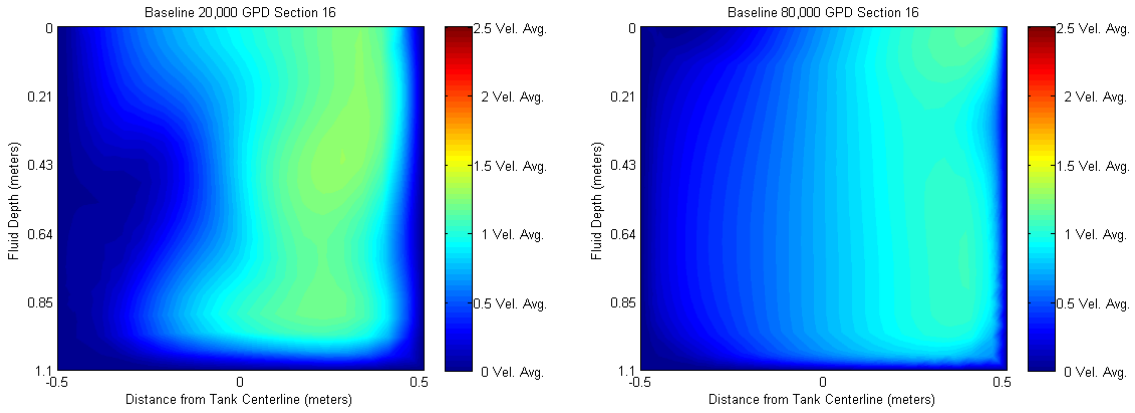

(a) 20,000 GPD **(b)** 80,000 GPD

Figure 4.18: Velocity profiles at section 16 for the tee inlet

lower the maximum velocities in the flow; encourage a uniform flow field; and discourage the formation of the downstream jet. Figures 4.19 and 4.20 show that this inlet achieved all of these design criteria, which allowed it to increase the tank efficiency by as much as 17%.

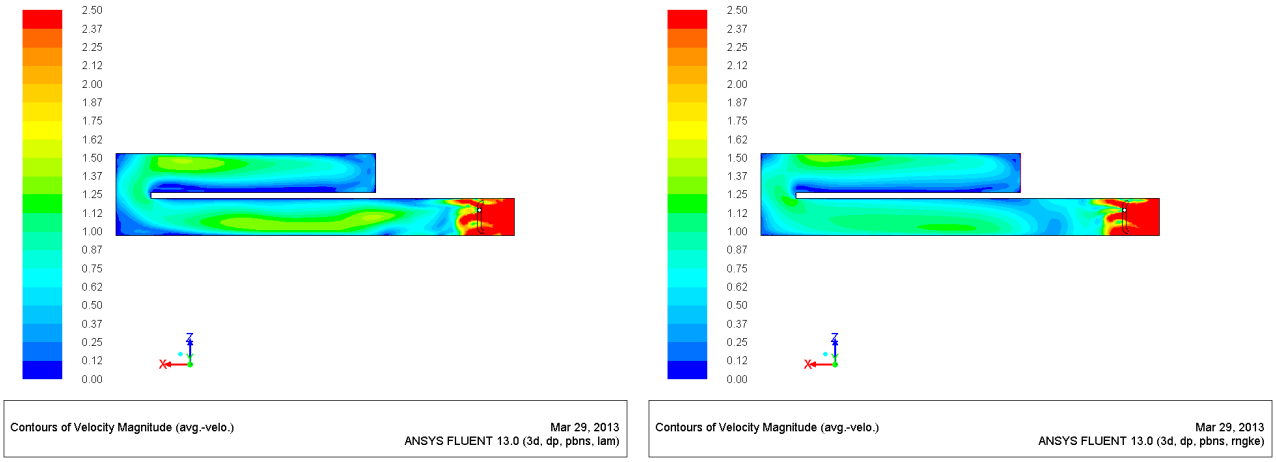

(a) 20,000 GPD **(b)** 80,000 GPD

Figure 4.19: Velocity profile 0.1 meters off tank bottom for the tee inlet

Table 4.4 shows how the different inlet modifications affected the baffle factor of the tank. This table helps further demonstrate that when the tank is operating at higher flow rates, the baffle factor is not significantly affected by inlet modifications. Since the tank is operating under a laminar flow regime during the low flow rates, there is very little mixing

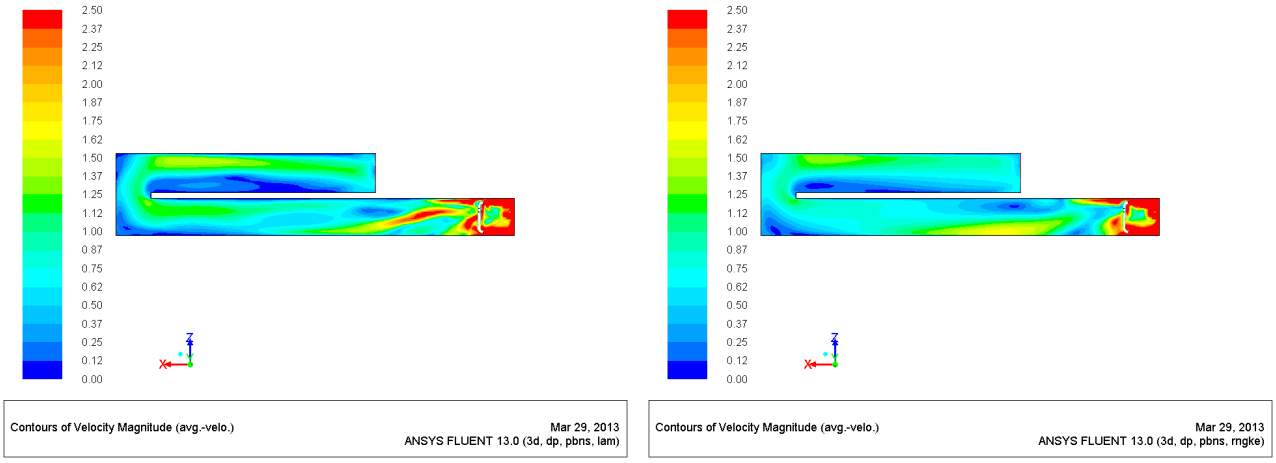

(a) 20,000 GPD **(b)** 80,000 GPD

Figure 4.20: Velocity profile 0.5 meters off tank bottom for the tee inlet

Table 4.4: Summary of CFD results

	20,000 GPD		80,000 GPD	
Inlet Condition	Baffle Factor	Percent Increase	Baffle Factor	Percent Increase
Baseline	0.52	0.00%	0.63	0.00%
90° Elbow	0.56	7.69%	0.65	3.17%
Tee Manifold	0.62	19.23%	0.67	6.35%
Idealized	0.67	28.85%	0.75	19.05%

occurring and there are large stagnation zones near the walls.

4.5.2 Installation and Tracer Studies of System Modifications

At the time of this writing, only the 90° elbow modification had been installed and tested. This elbow was attached to a 6″ pipe that was then placed over the original 4″ inlet. Once this modification was installed a lithium tracer study was performed with a flow rate of 20,000 GPD to validate the CFD model. Figure 4.21 shows the results of this tracer study. As this figure shows, the 90° elbow modification was able to increase the *BF* of the system to 0.61. Currently the tee manifold modification is being constructed and should be installed and tested early March 2013.

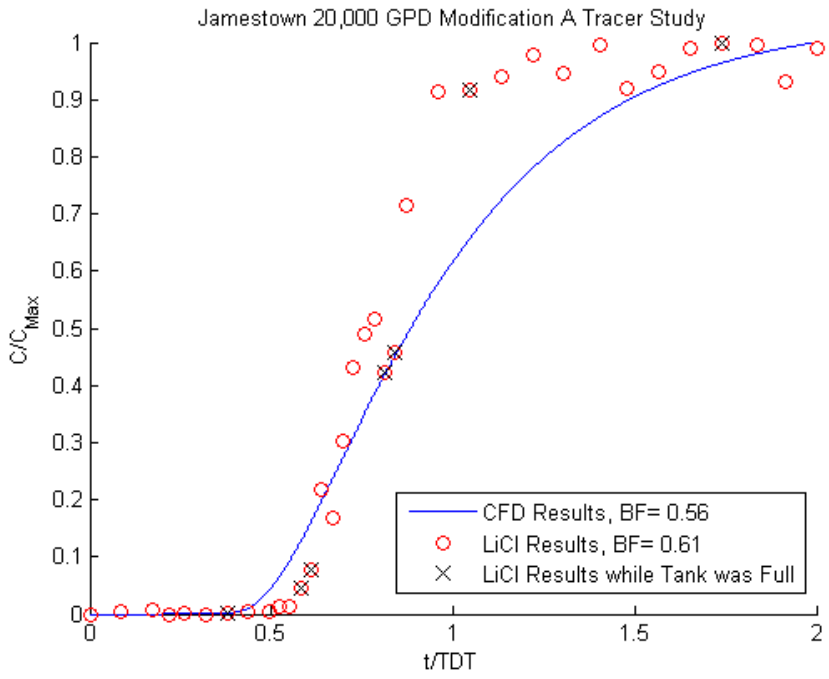

Figure 4.21: Tracer result for the 90° elbow modification

4.6 Conclusions

When serpentine contact tanks are designed they are usually most effective if they have a large length to width ratio Taylor (2012). However this design parameter has been derived from CFD simulations and experiments in which the flow is turbulent. In a turbulent flow energy is dissipated much quicker than in laminar flow. This case study highlighted the importance of turbulent mixing within water contact tanks. This aspect has been neglected in many design manuals. As this case study showed, the Jamestown contact tank performed very well during the high flow rates for which it was designed. However when the flow rates were less than 1/9 of the design flow rate, the tank was no longer functioning as intended. The CFD models showed that with simple inlet modifications the variability in BF of the system between the high and low flow rates could be reduced to only an 8% change.

Without the dissipation effects caused by a turbulent flow, an internal jet was able to form which caused the tank to perform poorly. This reduction in the baffle factor of the

contact tank, coupled with the much lower water temperatures during the winter months, necessitated the use of additional chlorine. While the chlorine levels were still within limits tolerated by the EPA, it still caused problems for the plant. Since the plant needed higher chlorine levels, it unnecessarily raised their operating cost. The raised chlorine levels also put the plant at risk for having higher levels of disinfection by-products (DPBs). Once the proposed modifications to the contact tank are installed and the results have been verified, less chlorine will be needed to treat the drinking water. This reduction in chlorine usage will benefit the plant in the long term by allowing for lower operating costs.

Chapter 5

Simple Internal Tank Modifications

5.1 Introduction

While internal baffling can greatly improve the efficiency of a contact tank, it is not always feasible or practical to use. Internal baffling can also be costly to install after a tank has been constructed. To further complicate the installation of internal baffling, it is not unusual for small water systems to use prefabricated storage tanks as a contact tank. These prefabricated storage tanks are typically made of plastic and come in shapes that are not conducive for internal baffling to be installed. While these plastic storage tanks are inexpensive compared to concrete tanks, they perform poorly as shown by Taylor (2012) and Wilson (2011). Several inlet modifications and random packing material were investigated in an effort to improve these storage tanks. All the models in this chapter assumed that the storage tank will be used as a water contact tank only and thus had a constant flow depth.

5.2 Computational Methodology

The CFD models presented in this chapter were set up in a manner very similar to those outlined in Section 3.2. For the simulations in this chapter the RNG k-ϵ turbulence model with the enhanced wall function was used to handle the turbulence closure issue from the RANS Navier-Stokes equations. The RNG k-ϵ turbulence model was chosen over the Standard k-ϵ model due to its ability to handle swirling flows (ANSYS, 2011). However extra steps were taken to ensure that the flow field was fully converged before the passive scalar was tracked as it progressed through the system. While the simulations in Chapters 3 and 4 consisted of

two steps, the ones presented in this chapter have three. First, the steady-state velocity field was calculated to reduce any issues with the transient model. Next the transient solver was used to calculate the transient velocity field out to a flow time of 2 TDT before the scalar was introduced into the simulation. This extra transient step was necessary as fluctuations in the RTD curve were noticed when a two-step model was used. These fluctuations of the RTD curve were indicative of a system which had a velocity field that was still developing.

5.3 Inlet Modifications

A 400-gallon doorway tank was chosen for the inlet parametric study. This tank was selected because it has become popular with many small water providers. Due to the geometry of the tank, it is able to easily fit through most standard doorways and hallways. Figure 5.1 shows the doorway tank that was installed in CSU ERC Hydraulics Lab.

The parametric study with the doorway tank looked at three different inlet configurations, two different inlet sizes, and a variety of flow rates ranging from 5 to 30 GPM. These inlet modifications would be kept as simple as possible so that a plant operator would be able to install them without any issues. It should be noted that the two holes through the tank in Figure 5.1 are not used to increase the tanks efficiency. Instead these holes are needed structurally to keep the tall flat sides from bowing out when the tank is full. While the original design of the holes was for a purely structural purpose, they do affect the internal velocity fields.

5.3.1 Model Geometry

It was decided that three different inlet conditions would be modeled for the parametric study: a sharp inlet (Case A); a tee (Case B); a 90° elbow pointing downward (Case C). Figure 5.2 shows the three different inlet conditions. Each case was modeled with two inlet diameters (1.75″ and 2.25″). These options were selected for the study because they were

Figure 5.1: Doorway tank as installed at CSU's ERC hydraulic laboratory

all inexpensive to implement and would be easy for any plant operator to install.

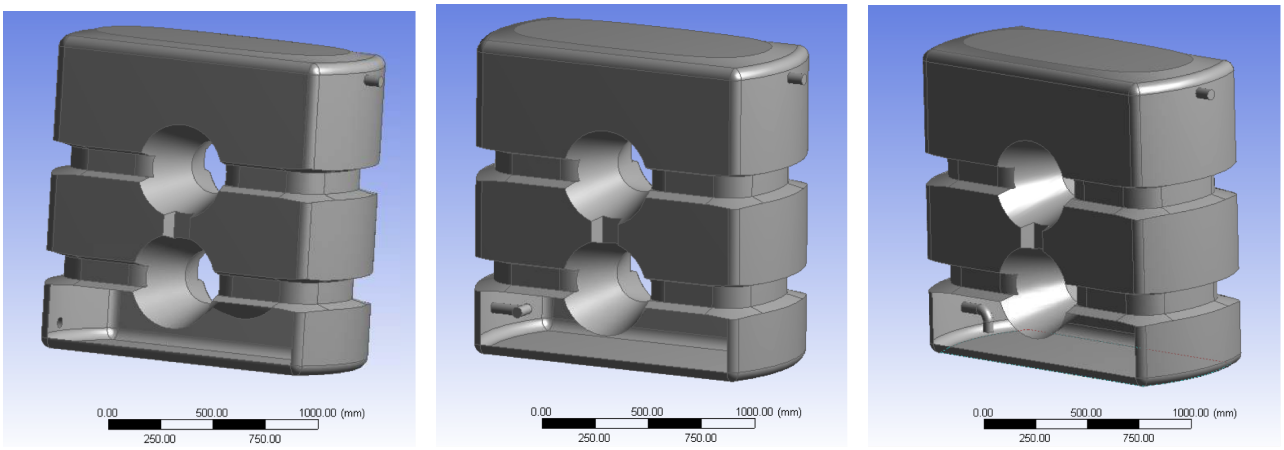

(a) Case A: straight **(b)** Case B: tee **(c)** Case C: 90° elbow

Figure 5.2: Model geometries for the parametric inlet study

Before a parametric study on different inlet modifications could be performed, the water surface elevation (WSE) within the tank needed to be determined. Unfortunately the license

for FLOW-3D had not been acquired at this stage in the project so the two-phase model in FLUENT was used. This two-phase model was initialized with a starting water surface of 4″ and a flow rate of 20 GPM. Since the inlet size would have no effect on the final WSE only the 1.75″ inlet diameter was modeled. The transient model in FLUENT was then used to fill the tank while the effluent rate was monitored at the outlet. This model then converged on the WSE when the effluent monitor at the outlet had reached a steady state and equaled the influent rate. The two-phase model showed that the fluid depth within the doorway tank was approximately 5 feet. All of the model geometries were then edited so that they reflected this fluid depth.

5.3.2 Model Meshes

Since each of the proposed inlet conditions would generate very different velocity fields a parametric mesh study was performed for all three cases. These parametric mesh studies used only the meshes that had an inlet size of 1.75″ because this inlet size would generate the highest velocities. The mesh was considered appropriately sized if the maximum velocities found in the studies were converging. Each mesh was created using ANSYS Workbench version 13. A smooth transition inflation layer was enforced on all of the walls so that the y^+ values would be within the proper range for the enhanced wall function. The inlets were treated as a velocity inlet while the outlet was treated as a pressure outlet discharging to the atmosphere. The turbulent kinetic energy (k) and turbulent kinetic energy dissipation rate (ϵ) were also specified for the inlet and outlet using the formulas found in the ANSYS *Theory Guide* and varied depending on the inlet size and the system flow rate. The water surface was then treated as a symmetry boundary. Figure 5.3 shows the results of each of the parametric studies. All of the meshes were considered acceptable since all of the maximum velocities were within 0.05 m/s. Since the meshes were all acceptable the medium mesh option was chosen for Cases A and B while the finest mesh was selected for Case C.

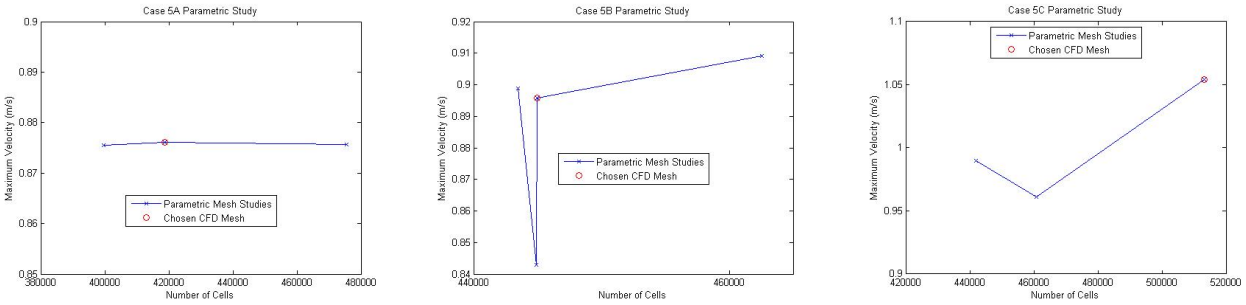

(a) Case A parametric results **(b)** Case B parametric results **(c)** Case C parametric results

Figure 5.3: Parametric results of mesh sizing for the doorway tank

5.3.3 Tracer Results

Before the CFD results were interpreted, they were verified using a step input tracer study. For more detail on step input tracer studies please see Section 2.3.2. Figure 5.1 shows how the doorway tank was set up during the tracer studies. This installation was the same as Case A with a 1.75″ straight inlet into the bottom of the tank. The outlet where the samples were taken was 2.25″ in diameter and located on top of the tank across from the inlet. With the tank plumbed in this manner it can only be used as a contact tank, however many times this type of tank will be used as a dual contact/storage tank. When the tank is used for this dual purpose, the plumbing is swapped with the inlet at the top and the outlet at the bottom. However when the tank is plumbed for dual purpose the water surface can vary if the inlet and outlet are not operating at the same flow rate. This creates a truly transient system unlike the quasi steady state that was modeled, and as such it was outside of the scope of this study.

As Figure 5.4 shows the lithium tracer studies closely match the CFD data. FLUENT was not only able to accurately predict the baffling factor of the system, but also correctly modeled the RTD curve. It is important that these two parameters match. Many times, different systems will have baffling factors that are very similar, yet have RTD curves that are drastically different. These three lithium tracer studies not only validated the CFD

simulations for Case A, but also Case B and C. This is because each case used a mesh that was selected based on a parametric mesh study. Figure 5.4 validates this method for selecting an appropriate mesh resolution.

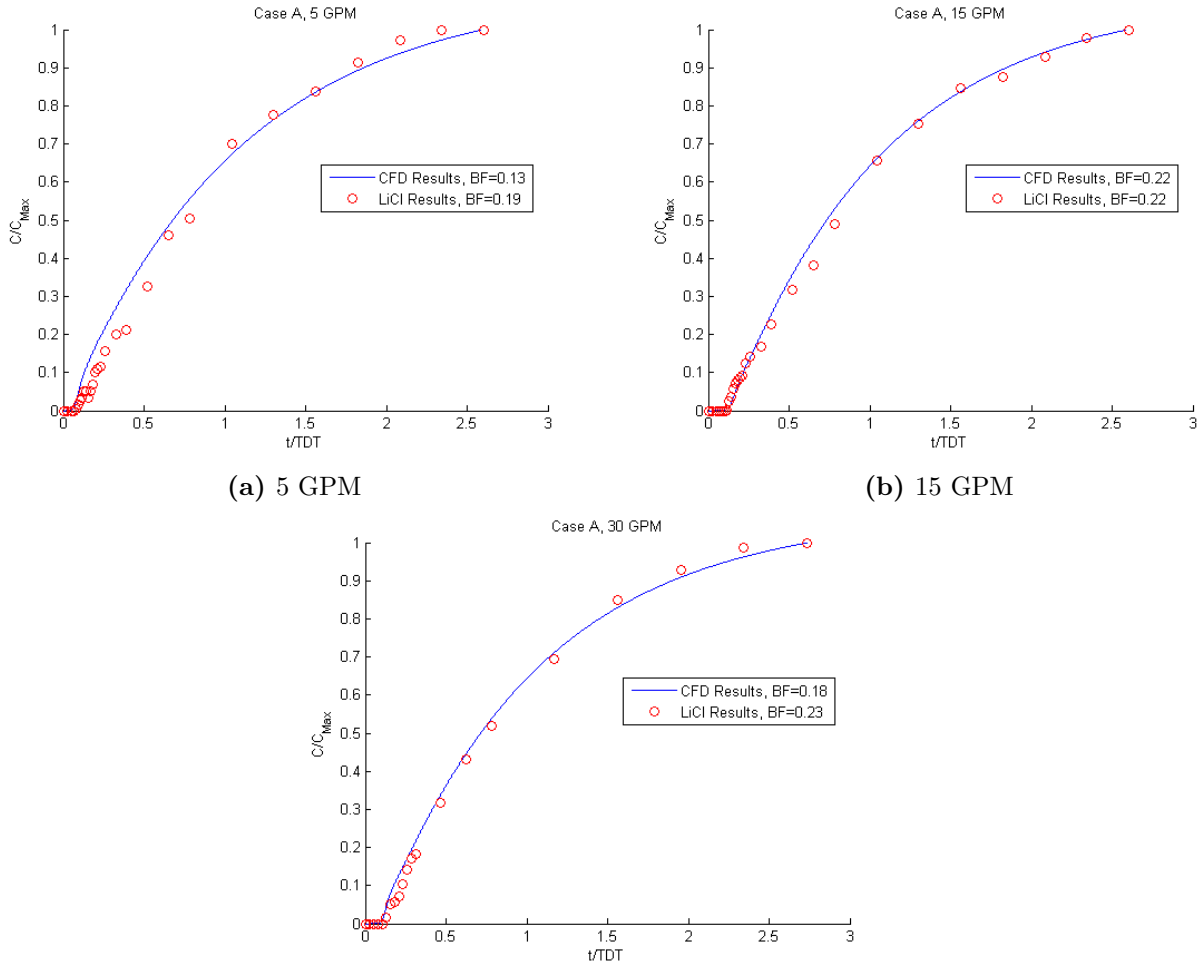

(a) 5 GPM

(b) 15 GPM

(c) 30 GPM

Figure 5.4: Lithium results for Case A, inlet size = 1.75″

5.3.4 CFD Model Results

A total of 6 flow rates (5 GPM, 10 GPM, 15 GPM, 20 GPM, 25 GPM, and 30 GPM, respectively) were modeled for each inlet condition to study how the baffle factor of the tank varied with flow rate. This parametric study was repeated with an inlet size of 1.75″ and

2.25″ so that a relationship between inlet sizes could be established. In total this parametric study had 36 high-resolution computer simulations. Figure 5.5 shows how the baffle factor varies with the flow rate for the three different cases. As Figure 5.5 shows, the 2.25″ inlet consistently outperforms the smaller 1.75″ inlet.

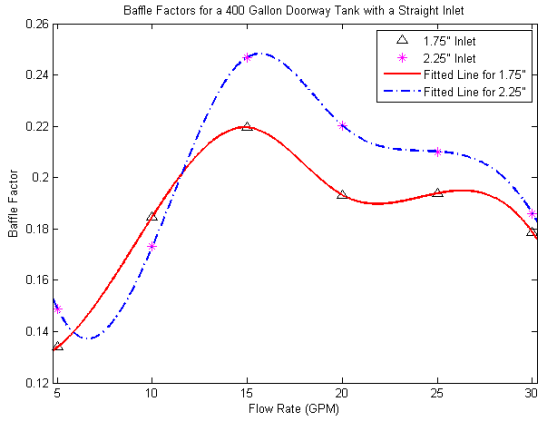

(a) Case A: straight

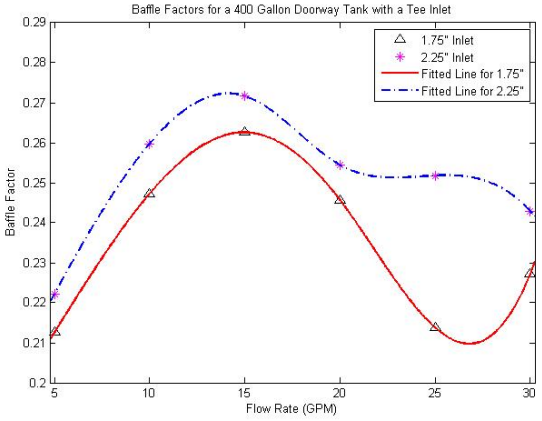

(b) Case B: tee

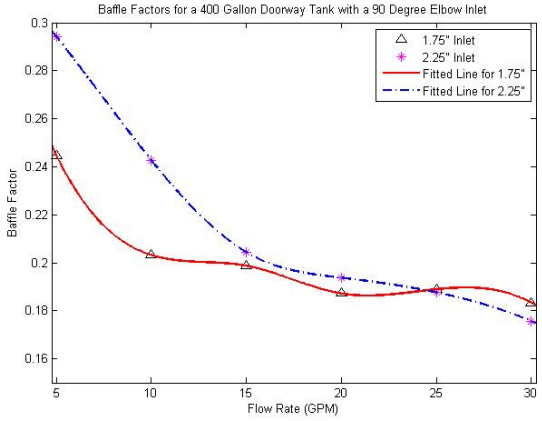

(c) Case C: 90° elbow

Figure 5.5: Baffle factor results

This trend was very interesting as it allowed the baffling factor to change by as much as 16% with only the size of the inlet being changed. Figure 5.5 also suggests that the inlet orientation/shape is able to greatly change the internal flow dynamics of the tank. To provide further insight into how the inlets influence the internal hydraulics, the average velocities of each simulation and the percent difference between them were calculated and are shown in

Table 5.1. This table shows that as the flow rate through the system increases, so does the average velocity. However, in almost every simulation, the tank with a 2.25″ inlet opening had average velocity that was around 23% lower than its 1.75″ counterpart. As a contact tank becomes more hydraulically efficient the amount of eddies and dead zones within the tank decrease. This decrease in dead zones and eddies will cause a lower average velocity within the tank as more of the tank volume is being utilized. The percent differences in the average velocities between the two inlets sizes found in Table 5.1 agree with the results shown in Figure 5.5.

Table 5.1: Average velocities (ft/min) of doorway tank

Flow Rate	Case A			Case B			Case C		
	Inlet Size		Percent	Inlet Size		Percent	Inlet Size		Percent
(GPM)	1.75″	2.25″	Difference	1.75″	2.25″	Difference	1.75″	2.25″	Difference
5	1.11	0.83	25.3%	0.35	0.30	13.4%	0.46	0.34	26.5%
10	2.28	1.72	24.2%	0.67	0.56	16.1%	1.18	0.86	26.3%
15	3.63	2.78	23.4%	1.10	0.85	22.7%	1.88	1.41	25.0%
20	4.97	3.80	23.5%	1.59	1.19	25.4%	2.59	1.92	26.0%
25	6.30	4.81	23.6%	2.03	1.56	23.1%	3.29	2.51	23.7%
30	7.62	5.83	23.5%	2.69	1.94	28.0%	4.01	3.01	24.8%

However Table 5.1 alone does not explain why the trends between the inlet modifications differ so drastically. To investigate further, the average velocity field along the mid plane of the doorway tank was plotted for several key simulations. Figure 5.6 shows 6 of these velocity fields. Figures 5.6a and 5.6b show the mid plane velocity contours of the straight inlet at 15 GPM. The jet that occurs from this inlet condition goes directly across the bottom of the tank before it bounces off of a wall. While the jet in these two figures looks identical, it disperses quicker with a 2.25″ inlet as shown in Figure 5.6b. Figures 5.6c and 5.6d show the mid plane velocity profile for the tee inlet at 25 GPM. The two jets created by this inlet condition are quickly dispersed in both cases since they are directed at the sidewalls. Most of the flow then travels along the bottom of the tank and up the back wall, however some travels up the front wall and across the top of the tank. Figures 5.6c and 5.6d along with Table 5.1

explain why the tee inlet condition was the best overall case. With this inlet condition the initial jets from the inlet are quickly dissipated. Then the flow splits into two streams, one along the floor of the tank and one along the front wall. These two flow paths help eliminate almost all of the tanks' dead zones. Finally, Figures 5.6e and 5.6f show the same velocity profile for the 90° elbow at 5 GPM. At this flow rate the 90° elbow inlet outperformed every case, however at flow rates higher than 5 GPM it did very poorly. Figures 5.6e and 5.6f show that the flow field caused by this inlet condition forms a larger area of high velocity near the inlet. While the 90° elbow caused most of the tank to be utilized, it allowed a large dead zone to form directly above the inlet. This dead zone was the primary reason why this inlet condition preformed so poorly.

5.3.5 Conclusion

Inlet conditions can greatly impact the internal hydraulics of a contact tank. Case B of the doorway tank study was the most effective over the widest range of flow rates. However this tee inlet allowed the baffle factor to fluctuate significantly depending on the flow rate within the system. It is not without surprise that Case B was the most efficient. Since the flow entered the system via two inlets, it did so with a much slower velocity than the single inlet systems. The average velocities in Table 5.1 confirm this. The larger 2.25″ tee inlet outperformed the smaller 1.75″ tee inlet for much the same reason. While the inlet diameter was only 22% bigger on the 2.25″ inlet, it had an inlet area that was 40% larger. This allowed the 2.25″ inlets in Case B to deliver the flow with 80% more inlet area than its 1.75″ counterpart.

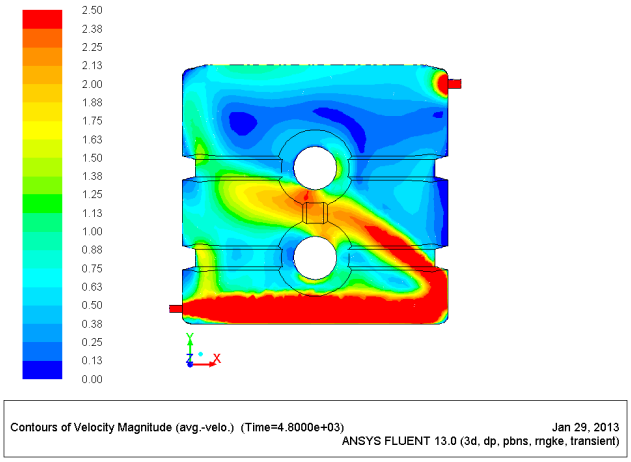

(a) Case A, 1.75″ inlet, 15 GPM

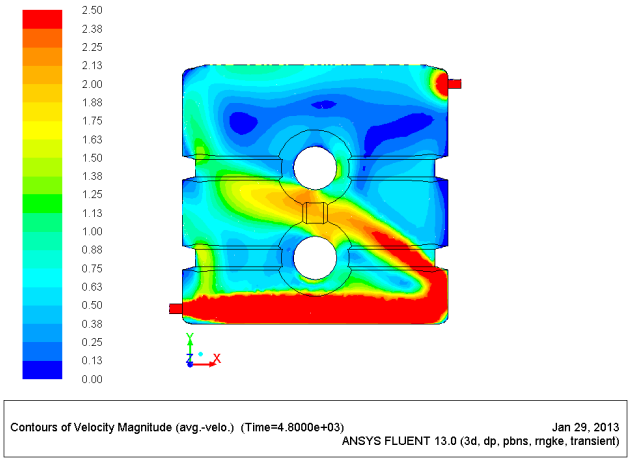

(b) Case A, 2.25″ inlet, 15 GPM

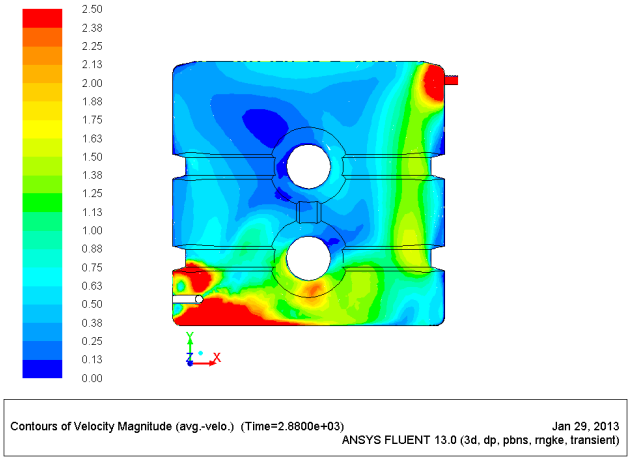

(c) Case B, 1.75″ inlet, 25 GPM

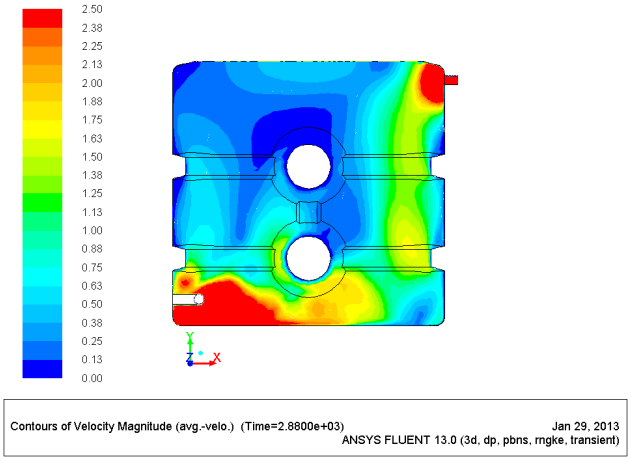

(d) Case B, 2.25″ inlet, 25 GPM

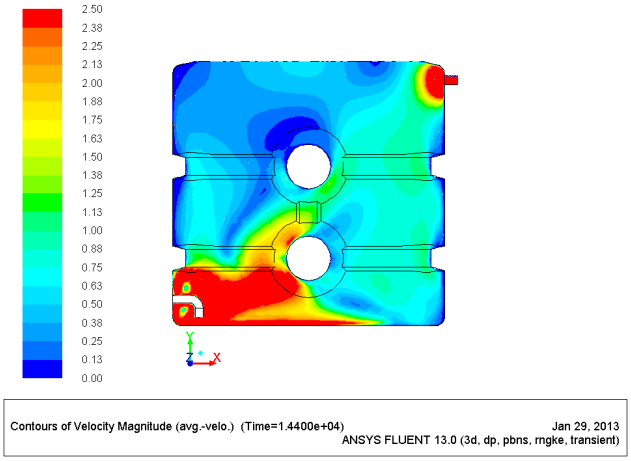

(e) Case C, 1.75″ inlet, 5 GPM

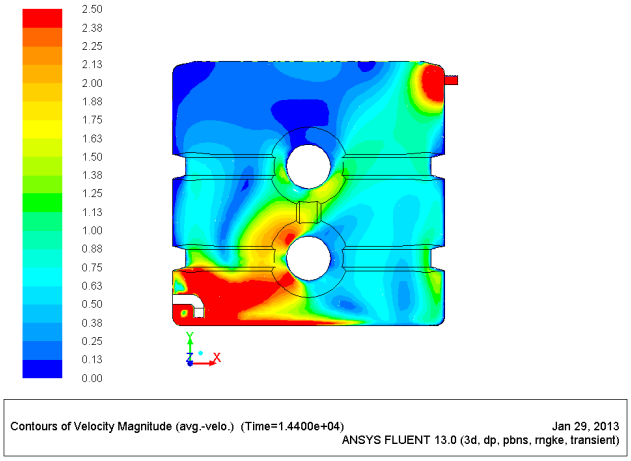

(f) Case C, 2.25″ inlet, 5 GPM

Figure 5.6: Average velocity profiles through the middle vertical plane

5.4 Packing Material

Packing material has long been used in vapor separation towers, however its use in water contact tanks has received little, if any, attention. This packing material is primarily designed to improve the efficiency of cooling towers or other applications were a vapor needs to be stripped from exhaust gases (RASCHIG JAEGER TECHNOLOGIES, 2006). Packing material is designed so that it can be poured into these towers (random packing) or where interlocking units are installed (structured packing). Companies that manufacture these packing materials have invested a significant amount of research and development to ensure that their product will outperform the competition.

However this research rarely looks into how the material changes the internal velocity profile in these towers. Instead companies design their product so that it will have the maximum usable surface area while minimizing any pressure losses within the system caused by the packing material structure. This design criteria yields products that have very similar characteristics regardless of manufacture or type of material (random or structured). Many types of packing material (both random and structured) are constructed out of material that has met National Sanitation Foundation (NSF) Standard 61 criteria, and as such are safe for applications in drinking water.

5.4.1 Methodology

Several different types of packing materials were investigated to determine applicability of use in water contact tanks. This study only investigated the use of random packing material due to the ease of installation in contact tanks. A 25-gallon tank was tested with $1''$, $2''$, and $3.5''$ random packing material at a flow rate of 5 GPM. This was scaled up to a 50-gallon tank that was used to investigate the same sizes of material at flow rates of 5 and 10 GPM, respectively. These tanks were supplied water via a $3/4''$ inlet at the bottom and had a $2''$

outlet located on top as shown in Figure 5.7. Figure 5.8 shows the three types of random packing material tested.

This packing material, while NSF 61 certified, did float and could have possibly been washed out of the system in the effluent. To prevent the material from escaping a mesh screen consisting of chicken wire with $3/4''$ openings was installed at the outlet. This mesh screen was installed prior to the baseline testing of the tanks so that any effect it would have on the baffle factor would be accounted for. The amount of material in these tanks was varied from 0%, 25%, 50%, and 100% of the tank volume. The tank volume lost to the packing material was negligible even when the tank was completely full as the void space of all of the sizes tested was 90% or higher. With this high void space the maximum tank storage volume lost was approximately 5 gallons. In total 64 saline tracer studies were performed in conjunction with several lithium tracer studies that were used to validate the saline results. Due to the highly complex and random nature of the packing material CFD simulations were not feasible.

To ensure the saline tracer results were accurate, each test was repeated a minimum of two times. The tracer stock solution was mixed so that it would raise the conductivity of the flow by 100 μC. As the effluent left the tank, some was diverted into a flow-through device as shown in Figure 5.7. This device was designed so that the flow would enter at the bottom and leave out the top. This configuration allowed for more accurate conductivity samples since no fluid could collect in the sampling area. Sampling times were based off of changes in the effluents conductivity since the RTD curve was not known apriori from CFD results. Once the conductivity at the outlet varied by less that 0.5 μC over a 5 minute period the test was stopped as the system had reached an equilibrium. However this equilibrium criteria lead to each test ending between 4 or 6 TDT's. To ease comparisons between each test, all of the data presented has been truncated to only 3 TDT. This truncation had little effect on the baffle factor of these systems.

Despite the precautions that were taken during these saline tracers, several anomalies still

Figure 5.7: Tanks used for packing tank study (25 gallon front, 50 gallon back)

Figure 5.8: Random packing material used

occurred. Since the hydraulics lab at the ERC used raw water from Horsetooth Reservoir, the background conductivity could vary from day to day. This variation was sometimes severe enough to induce shifts in the RTD curves generated by the saline results. To eliminate any error this might have caused, additional safeguards were taken. First, all of the results presented had minimum of two RTD curves that matched. This helped identify which tests had been compromised due to shifts in the background conductivity or other factors. The second step was that key tracer studies were repeated using a lithium solution.

5.4.2 Study Results: Lithium Tracers

Figure 5.9 shows the lithium tracer results of the baseline condition of the tanks. These baseline studies were conducted with the tanks empty of packing material, so that any improvements from the addition of the packing material could be compared. As Figure

5.9 shows the lithium results match well with the saline data. These initial tracer studies confirmed that the two different tanks initially had poor baffle factors, which ranged from 0.27 to 0.37.

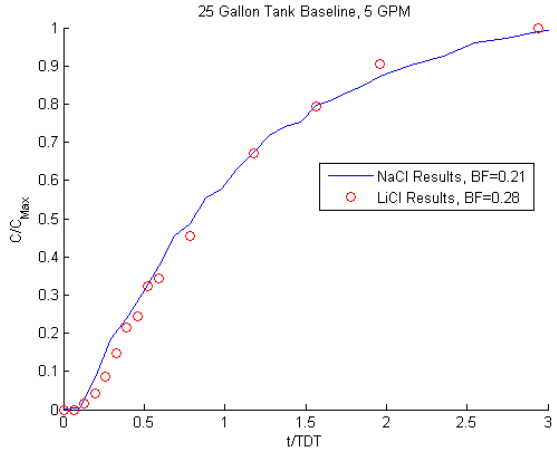

(a) 25 gallon tank, 5 GPM

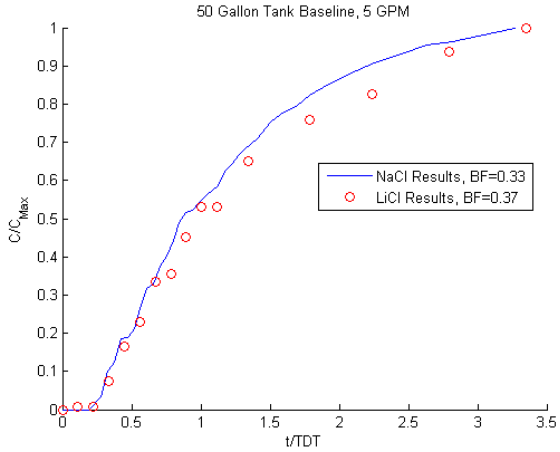

(b) 50 gallon tank, 5 GPM

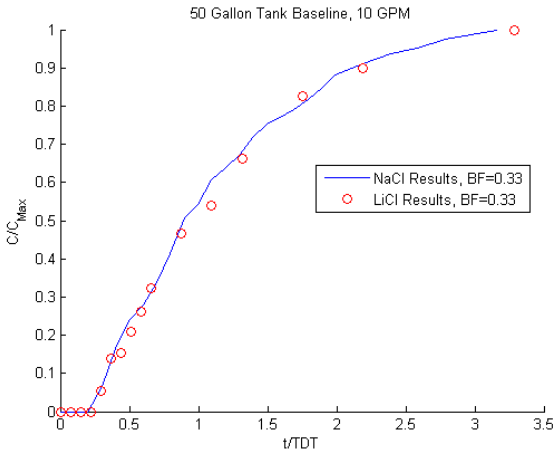

(c) 50 gallon tank, 10 GPM

Figure 5.9: Lithium baseline results

5.4.3 Study Results: $V_{Packing}/V_{Tank}$

During the tracer studies, the volume of packing material vs. tank volume ($V_{Packing}/V_{Tank}$) was varied to determine if there was an optimal ratio to use. The four different cases investigated were $V_{Packing}/V_{Tank} = 0\%$, 25%, 50%, and 100%. While all of the results showed

similar trends, only the 1-inch material in the 25-gallon tank is shown. Figure 5.10 shows the four RTD curves generated from the tracer study. As more packing material was added to the tank, the flow became more uniform and closer to plug flow. This trend was very linear as shown in Figure 5.11. The linear increase in the baffle factor as shown in Figure 5.11 was most likely caused by the material properties of the packing material itself. Since the packing material was lighter than the water, most of it was not near the inlet. Instead it would float at the top of the tank near the outlet. As more material was added into the tank, the interface between the tank volume containing the packing material and tank volume without packing material moved closer to the inlet. This allowed the packing material to disperse any jets or eddies caused by the inlet much quicker, which in turn allowed for more usable tank volume. If the packing material was heavier than water this trend might not hold.

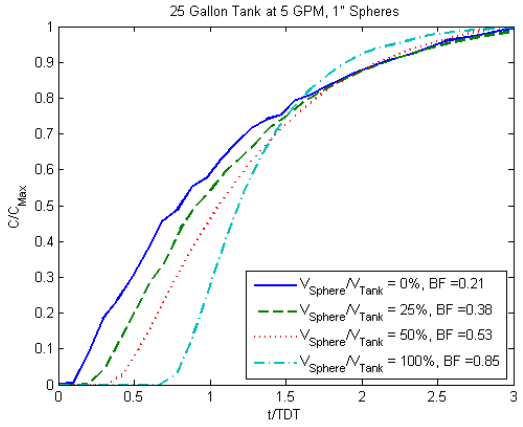

Figure 5.10: RTD curves from for 1″ packing material in a 25-gallon tank

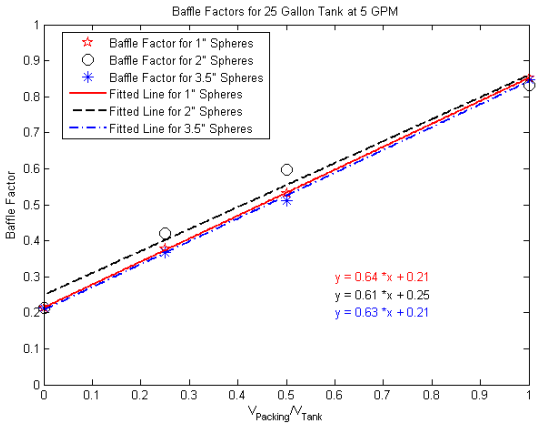

Figure 5.11: *BF* for the three material sizes with different $V_{Packing}/V_{Tank}$ values

5.4.4 Study Results: Material Size

These tracer studies revealed that the performance of the system was fairly independent of the packing material size. Figure 5.12 shows the RTD curves of the two tanks when $V_{Packing}/V_{Tank}$=100%. As this figure shows there is a slight variation between packing sizes,

however the baffle factor varied at most 15% between the different material sizes.

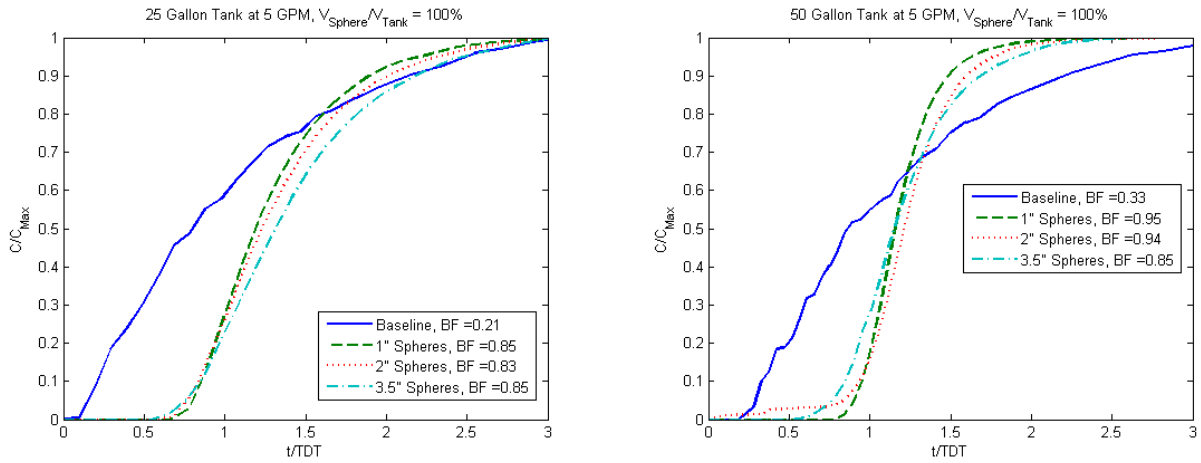

(a) 25 gallon tank

(b) 50 gallon tank, 5 GPM

Figure 5.12: RTD curves with $V_{Packing}/V_{Tank}$=100%

5.4.5 Study Results: Tank Size and Flow Rate

The increases seen in the 25-gallon tank with a flow rate of 5 GPM also scaled to the 50-gallon tank at both flow rates as seen in Figure 5.13. As Figure 5.13 shows there is no clear effect of tank size or system flow rate. However it is of interest that while the RTD curves in Figure 5.13a are very similar, they begin to separate in Figure 5.13b. This was most likely caused by the floatation of the packing material. As more packing material was added to the tank, more of the material was forced closer to the inlet. This allowed the material to disperse any jets caused by the inlet sooner. Since any jets or eddies were dispersed sooner it allowed for more volume of the tank to be usable.

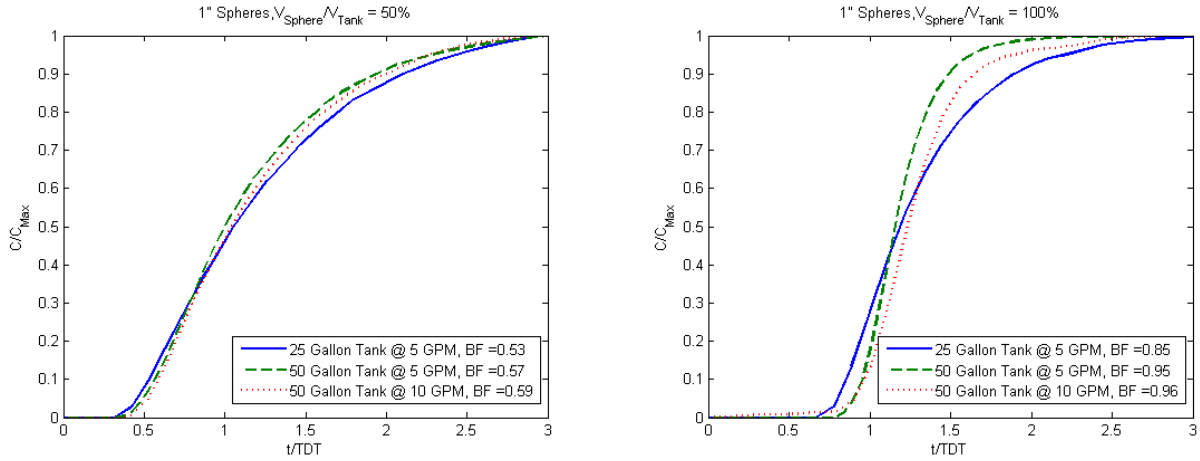

(a) $V_{Packing}/V_{Tank}$=50% **(b)** $V_{Packing}/V_{Tank}$=100%

Figure 5.13: RTD curves for 1″ material

5.4.6 Conclusion

Figure 5.14 shows the trend lines of the 1-inch spheres for the 25-gallon tank at 5 GPM and the 50-gallon tank at 5 and 10 GPM. As Figure 5.14 shows there is no tail off the increase of baffle factor with the use of this material. While the linear trends shown in Figure 5.14 are insightful, they are all basically the same. Each of the three lines have almost the exact same slope with the main difference being in where they cross the y-intercept. Figure 5.14 also shows that in the current study the material performance is independent of the system flow rate. Both the trend lines for the 50-gallon tank at 5 and 10 GPM have a slope and y-intercept that are within 3.5% of each other. These trend lines also show that the tank size could have a larger impact on the performance curve of the system. The primary difference between the 25 and 50-gallon trend lines was caused by the baseline performance of the tank.

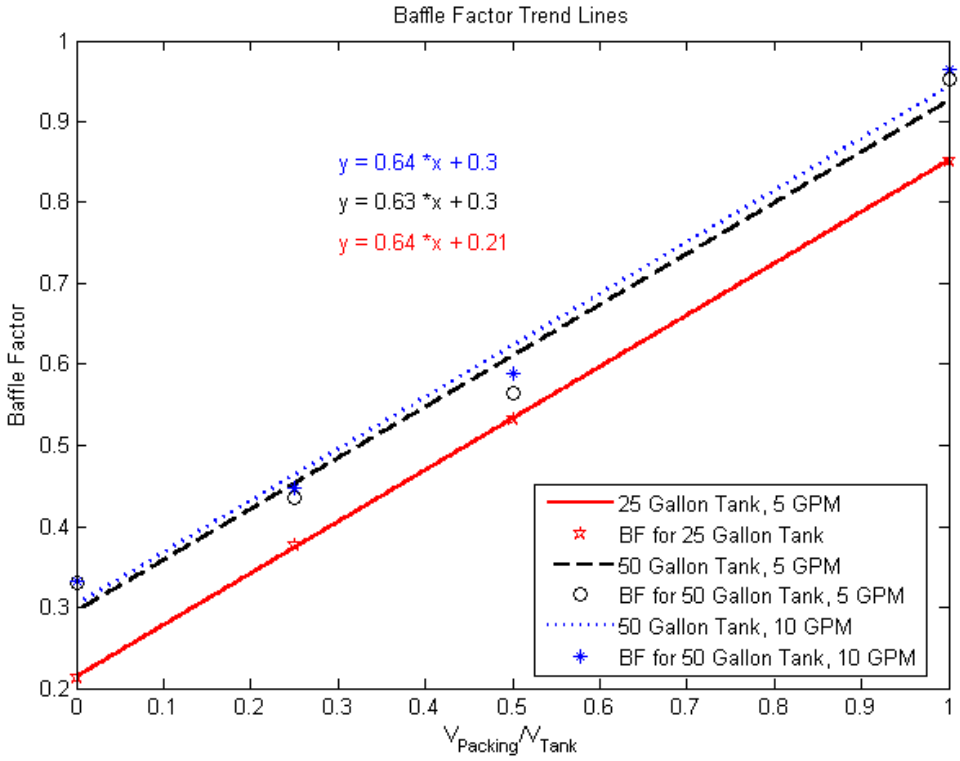

Figure 5.14: Trend lines of 1″ material for all tanks

5.5 Chapter Conclusions

The results presented in this chapter show that *BF* of water storage tanks can easily be increased through simple internal modifications to the tank. The most cost effective and easiest of these are inlet modifications, as they can be constructed and installed by the plant operator. Results from the inlet modification study showed that a well-designed inlet should disperse the flow quickly and effectively. This can be achieved through the use of a larger inlet or by modifying the inlet design itself. However, these inlet modifications fall short of the gains seen with the introduction of random packing material. This packing material is more costly than the inlet modifications and could cause issues when the tank is cleaned. Despite these issues with the packing material, its ability to quickly and evenly disperse the flow within a tank is unparalleled.

Chapter 6

Summary and Conclusions

6.1 Summary of Research

The research conducted and presented in this thesis used both CFD and physical tracer studies to further investigate the internal flows of drinking water contact tanks. The tracers studies performed further validated two different commercial CFD software packages, by proving that both CFD software packages could accurately track a passive scalar as it propagated throughout the contact tank.

Chapter 3 presented a parametric serpentine baffle tank study that used over 50 different baffle configurations with a fixed tank footprint. This parametric study further validated the work by Taylor (2012), while also provided new insights into the hydraulics of baffle tanks. Chapter 4 of this thesis consisted of a case study that was performed using the chlorine contact tank in Jamestown, Colorado. This case study highlighted the ability of CFD models to accurately model contact tanks and how CFD can be used as a design tool for future modifications. Chapter 5 investigated internal tank modifications that could be easily installed in pre-existing systems. This was achieved with 36 CFD models and over 70 tracer studies that were conducted using various tanks.

6.2 Major Conclusions

The serpentine baffle study presented in Chapter 3 showed that these tanks are most efficient when L^* is close to 20%, L_{bo}/W_{ch} is close to 1, and the length to width ratio of the baffle channels is maximized. This parametric study showed that flow separation and improper

channelization of the flow were the primary two hydraulic issues within these tanks. If the baffles had a L^* of 50% or higher, the flow would form a channel in the center of the tank and leave large dead zones or eddies. Alternatively the flow would separate around the baffle tips if the baffles had a L^* less than 20%. This flow separation would cause eddies near these baffle tips, which would in turn reduce the hydraulic efficiency of the tank.

The case study in Chapter 4 found that turbulent to laminar flow regime changes can cause a system to perform drastically different. This laminar/turbulent regime change is rarely mentioned in the context of drinking water contact tanks, however the effects it has are very important. In the case of the Jamestown contact tank, this regime change caused a 17.7% reduction in the efficiency of the system. With the use of CFD, two proposed inlet modifications were developed and were capable of improving the BF of the system by almost 17% while keeping the variability in the BF of the system within 8%.

The internal tank modifications in Chapter 5 were split into two categories (inlet modifications and packing material). The inlet modifications showed that with very simple changes the baffle factor could be improved by a maximum of 40%. This study also highlighted the importance of reducing the average velocity within a contact tank. This was achieved by using larger tee inlets. Since this larger tee inlet had more inlet surface area, it could deliver the influent at a slower velocity. This slower inlet velocity meant that any jets formed by the inlet were dispersed sooner, and hence yielded a lower average velocity within the tank. The packing material that was also investigated in this chapter showed that its use could greatly increase the efficiency of a system. This material was able to increase the baffling factor by up to 300% and achieved a maximum BF of 0.97. On average this material was able to increase the BF of a tank by 190% to 290% depending on the initial BF of the tank.

6.3 Recommendations for Future Work

Research is an ongoing and never ending process. As such, the following recommendations are being made for the continuing this research study.

- Parametric serpentine baffle study, similar to the one presented in this thesis, with the baffling rotated 90°. It is hypothesized that this will yield similar results and will help complete the baffling guidelines. This study should also include tracer studies that replicate the CFD models using the concrete tank in the CSU ERC Hydraulics Lab.

- Further work needs to be completed using the packing material. The material size, tank size, and system flow rate should continue to be increased until the effects from the packing material begin to taper off. The systems tested in the current research only provide an insight into very small contact tanks with a low flow rate and small packing material.

- Two phase CFD studies with variable influent and effluent are needed to investigate how this will affect the BF rating of a system. These two-phase systems will be able to more accurately predict the dynamics of a system, as these contact tanks rarely operate at the steady state that was modeled in the current research.

References

2006. *Product Bulletin 600.* RASCHIG JAEGER TECHNOLOGIES, Houston, TX.

2011. ANSYS FLUENT Theory Guide.

2012. *FLOW-3D Users Guide.* FLOW Science, Santa Fe, NM.

Amini, R., Taghipour, R., & Mirgolbabaei, H. 2010. Numerical Assessment of Hydrodynamic Characteristics in Chlorine Contact Tank. *Inernational Journal for Numerical Methods in Fluids.*

Baawain, Mahad S., El-Din, Mohamed Gamal, & Smith, Daniel W. 2006. Computational Fluid Dynamics Application in Modeling and Improving the Performance of a Storage Reservoir Used as a Contact Chanbed for Microorganism Inactivation. *Journal of Environmental Engineering and Science*, **5**, 151–162.

Davis, M. L. 2008. *Introduction to Environmental Engineering.* McGraw Hill.

EPA, US. 2004 (June). *Understanding the Safe Drinking Water Act.* Tech. rept. EPA 816-F-030. United States Environmental Protection Agency.

EPA, US. 2011 (July). *National Characteristics of Drinking Water Systems Serving Populations Under 10,000.* Tech. rept. EPA 816-R-10-022. United States Environmental Protection Agency.

Falconer, R. A., & Ismail, A.I.B.M. 1997. Numerical Modeling of Tracer Transport in a Contact Tank. *Environmental International*, **23**(6), 763–773.

Pope, Stephen B. 2010. *Turbulent Flows.* Cambridge University Press.

Rauen, William B., Lin, Binliang, Falconer, Roger A., & Teixiera, E. C. 2008. CFD and Experimental Model Studies for Water Disinfection Tanks with Low Reynolds Number Flows. *Chemical Engineering Journal*, **137**, 550–560.

Rauen, William B., Angeloudis, Athanasios, & Falconer, Roger A. 2012. Appraisal of Chlorine Contact Tank Modeling Practices. *Water Research*, **46**, 5834–5847.

Shiono, K. E., Teixiera, E. C., & Falconer, R. A. 1991. Turbulent Measures in Chlorine Contact Tank. *In: First International Conference of Water Pollution: Modeling, Measuring and Predicting.*

Taylor, Zachary H. 2012. *Towards Improved Understanding and Optimization of the Internal Hydraulics of Chlorine Contact Tanks.* Masters thesis, Colorado State University.

Venayagamoorthy, S. K., & Stretch, D. D. 2010. On the Turbulent Prandtl Number in Homogeneous Stably Stratified Turbulence. *Journal of Fluid Mechanics*, **644**, 359–369.

Versteeg, H K, & Malalasekera, W. 2007. *An Introduction to Computational Fluid Dynamics The Finitie Volume Method.* Second edn. Pearson Education Limited.

Wang, Hong, Shao, Xuejun, & Falconer, Roger A. 2003. Flow and Transport Simulation Models for Prediction of Chlorine Contact Tank Flow-Through Curves. *Water Environment Research*, **75**(5), 455–471.

Wilson, Jordan M. 2011 (Spring). *Evaluation of Flow and Scalar Transport Characteristics of Small Public Drinking Water Disinfection SYstems Using Computational Fluid Dynamics.* Masters thesis, Colorado State University.

Wilson, Jordan M., & Venayagamoorthy, Subhas K. 2010. Evaluation of Hydraulic Efficiency of Disinfection Systems Based on Residence Time Distribution Curves. *Environmental Science and Technology*, **44**, 9377–9382.

Xu, Qing. 2010. *Internal Hydraulic of Baffled Disinfection Contact Tanks.* Masters thesis, Colorado State University.

Zhang, Jun-Mei, Lee, Hoew Pueh, Khoo, Boo Cheong, Teo, Chit Pin, Haja, Nazarudeen, & Peng, Kai Qui. 2011. Modeling and Simulations of Flow Pattern, Chlorine Concentration, and Mean Age Distributions in Potable Water Service Reservoir of Singapore. *Journal of Environmental Engineering*, **137**(7), 575–584.

Zhang, Jun-Mei, Khoo, Boo Cheong, Lee, Hoew Pueh, & Teo, Chit Pin. 2012. Effects of Baffle Configurations on the Performance of a Potable Water Service Reservoir. *Journal of Environmental Engineering*, **138**(5), 578–587.

Appendices

Appendix A

User Defined Function For Diffusivity

This is the user defined function (UDF) that was used to define the diffusivity of the passive scalar in FLUENT.

```
/**************************************************************************
UDF that computes the diffusivity of mean age using a user-defined scalar
**************************************************************************/
#include "udf.h"
DEFINE_DIFFUSIVITY(diff_coeff,c,t,i)
{
return C_MU_T(c,t) / 0.7+0.001;
}
```